Astronomy & Astrophysics manuscript no.
(will be inserted by hand later)

Rotation curves and metallicity gradients from HII regions in spiral galaxies ⋆

I. Márquez[1⋆⋆], J. Masegosa[1], M. Moles[⋆⋆2], J. Varela[2], D. Bettoni[3], and G. Galletta[4]

[1] Instituto de Astrofísica de Andalucía (CSIC), Apartado 3004 , E-18080 Granada, Spain
[2] Instituto de Matemáticas y Física Fundamental (CSIC), C) Serrano 113B, E-28006 Madrid, Spain.
[3] Osservatorio Astronomico di Padova, Vicolo Osservatorio 5, 35122 Padova, Italy
[4] Dipartimento di Astronomia, Università di Padova, Vicolo Osservatorio 2, 35122 Padova, Italy

Received: ; accepted:

Abstract. In this paper we study long slit spectra in the region of Hα emission line of a sample of 111 spiral galaxies with recognizable and well defined spiral morphology and with a well determined environmental status, ranging from isolation to non-disruptive interaction with satellites or companions. The form and properties of the rotation curves are considered as a function of the isolation degree, morphological type and luminosity. The line ratios are used to estimate the metallicity of all the detected HII regions, thus producing a composite metallicity profile for different types of spirals. We have found that isolated galaxies tend to be of later types and lower luminosity than the interacting galaxies. The outer parts of the rotation curves of isolated galaxies tend to be flatter than in interacting galaxies, but they show similar relations between global parameters. The scatter of the Tully-Fisher relation defined by isolated galaxies is significantly lower than that of interacting galaxies. The [NII]/Hα ratios, used as metallicity indicator, show a clear trend between Z and morphological type, t, with earlier spirals showing larger ratios; this trend is tighter when instead of t the gradient of the inner rotation curve, G, is used; no trend is found with the interaction status. The Z-gradient of the disks depends on the type, being almost flat for early spirals, and increasing for later types. The [NII]/Hα ratios measured for disk HII regions of interacting galaxies are higher than for normal/isolated objects, even if all the galaxy families present similar distributions of Hα Equivalent Width.

Key words. Galaxies: spiral – kinematics and dynamics – structure – interaction

1. Introduction

The analysis of the rotation curves of disk galaxies is the most direct way to obtain information on the mass distribution of spiral galaxies. The ionized gas has been used for long as a tracer of their kinematics. During the 80's, Rubin and collaborators started a systematic effort to obtain accurate rotation curves of spiral galaxies of all morphological types and luminosity (Rubin et al. 1991, and references therein). The accumulation of data from different sources helped to get an overall picture of the form of the rotation curve of spirals, and its relation with other galactic properties. It is now recognized that the maximum rotational velocity, V_m, is related with the total mass (and luminosity) of the galaxy, with the optical scale radius of the disk and with the morphological type (see Persic et al. 1996). The flatness of the outer rotation curve in most cases also led to accept the existence of massive dark halos in spiral galaxies (see Rubin et al. 1991; Sofue 1998).

Most of those analysis were based on data sets assembled with no completeness criteria. In particular, the galaxies were considered as field or cluster objects, and no further attention was payed to their environmental status, in spite of the expected influence of even small companions on the mass distribution, and star formation history of a given galaxy. Spiral galaxies in very close isolated pairs were studied by Keel (1993, 1996). Trying to understand the effects of the interaction on the dynamics of disk galaxies, Márquez & Moles (1996; hereafter Paper I) studied the properties of isolated (see below for the definition of isolation) spiral galaxies, to set a zero-point for the effects of the interaction; see also Mathewson et al. 1992, and Courteau 1997, for an analysis of field spirals).

Send offprint requests to: I. Márquez (*isabel@iaa.es)*

⋆ Based on data obtained Asiago/Ekar Observatory. Also based on observations made with INT operated on the island of La Palma by ING in the Spanish Observatorio del Roque de Los Muchachos of the Instituto de Astrofsica de Canarias.

⋆⋆ Visiting Astronomer, German-Spanish Astronomical Center, Calar Alto, operated by the Max-Planck-Institut fur Astronomie jointly with the Spanish National Commission for Astronomy

Márquez & Moles (1999; hereafter Paper II), studied also the properties of spirals in isolated pairs, and compared them to those of the isolated galaxies in Paper I. It was found that the main differences is the presence of type II disk profiles in interacting systems (but not in isolated galaxies), and a flatter outer rotation curve in isolated galaxies. No distorted curves were found among isolated disk galaxies.

More recently, 2D Fabry-Perot rotation curves have been obtained for a number of cluster spirals in order to determine the environmental effects in such large aggregates. The results show a complex pattern (Amram et al. 1996). Barton et al. (2000, 2001) have also analyzed the rotation curves of spiral galaxies in close pairs and in the general field in order to put some constraints on the cluster effects on the kinematical properties of galaxies, and the consequences in their use for distance estimation by means of the Tully-Fisher relation. Their results do confirm the earlier results in Paper II, in the sense of a more scattered T-F relation for non isolated objects. Similarly, galaxies with interacting companions in the recent analysis by Kannappan et al. (2002) fall on the high luminosity/low velocity width side of the TF and show more scatter.

We emphasize that the so called field galaxies should be carefully investigated since some of them could still be perturbed by small companions or satellites, that could produce significant effects (Athanassoula 1984; Conselice & Gallagher 1999; Conselice et al. 2000). In Paper I and II a quantitative criterion of isolation was given, trying to identify truly isolated objects to build up a reference for the analysis of the effects of gravitational interaction. We will use a similar approach here.

The same long slit spectroscopic data used for the study of the gas kinematics can also be used, through the flux ratios of the observed emission lines, to trace the metallicity, Z, along the disk, and to determine the existence of Z-gradients. The existing analysis point out that the global metallicity is related to the mass (hence, to V_m), and that Z decreases gently outwards (see the review by Henry & Worthey 1999). Ferguson et al. (1998) have extended the analysis towards the extreme outer regions of disks, finding that Z drops there abruptly, but keeping values far from pristine.

In the present paper, we will study a sample of 111 spiral galaxies with a well studied environmental status, ranging from isolation to mild interaction with satellites or companions. In all cases however the interaction is non disruptive (they have been selected to have recognizable and well defined spiral morphology). The data comprise new long slit spectroscopy for 85 spiral galaxies. The remaining data are from Paper I. The form and properties of the rotation curves are considered as a function of the isolation degree, morphological type and luminosity. The line ratios are used to estimate the metallicity of all the detected HII regions, thus producing a composite metallicity profile for different types of spirals.

Section 2 is devoted to the description of the sample and the determination of the interaction status. In Section 3, the observations and data reduction procedures are presented. Section 4 and 5 deal with the rotation curves and the Tully-Fisher relation, respectively. In Section 6 the properties of nuclear and extranuclear HII regions are described. The summary and conclusions are given in Section 7.

2. The sample

The 85 galaxies with new long slit data come from three sources:

- Automatically selected isolated galaxies from the CfA catalogue (Huchra et al. 1999), among those brighter than $m_B = 13$ (and not bigger than $4'$ in diameter, for practical reasons), with an inclination between 32°and 73°, to minimize the uncertainties with the correction in both, photometric and kinematic parameters. The isolation criterium for automatic selection was that they had no CfA companions (i. e., with known red-shift) within a projected distance of 0.5 Mpc, or with a red-shift difference greater than 500 km/s (see Márquez 1994; Paper I). A total of 43 galaxies were selected in that way
- An additional sample of 29 spiral galaxies also from the CfA catalogue, also imposing the automatical isolation criteria and with $|b| \geq 40°$but with no restrictions in apparent magnitude, size or inclination
- Thirteen spiral galaxies in 7 pairs taken from the catalogue of isolated pairs by Karachentsev (1972). We applied the automathic isolation criterium to the pair as a whole. In addition to this, only those galaxies with still recognizable and well defined morphology were retained. Therefore, we implicitly avoid strongly interacting galaxies, with about 40 % of pairs being widely separated, in contrast with previous studies of pairs of spirals, where mostly close pairs were selected (Keel 1993, 1996; Barton et al. 2001).

We have also included in our final sample a total of 26 spiral galaxies (17 isolated and 9 spirals in 5 S-S pairs) from Paper I[1], so the analysis refers to the whole sample of 111 spiral galaxies. Notice that since we imposed that the candidates would have a well defined spiral morphology, and no bright (CfA) companions, our sample does not include cases of very strong and/or disruptive interaction. Nevertheless, even in those mildly interacting systems the perturbations can be recognizable depending, other than on the properties of the galaxy itself, on the mass, size, distance and relative velocity of the perturbing agent.

[1] Isolated galaxies: NGC 818, UGC 3511, UGC 3804, NGC 2532, NGC 2712, IC 529, NGC 3294, NGC 3549, NGC 3811, NGC 3835, NGC 4162, NGC 4290, NGC 4525, NGC 5962, NGC 6155, NGC 6395, NGC 6643; spirals in Karachentsev's pairs: NGC 2798/99, NGC 4567/68, NGC 3646, NGC 7469/IC 5283, NGC 7537/41

2.1. The isolation status revisited

As a second step for defining a sample of isolated galaxies, the previously selected as isolated were investigated for the presence of perturbing companions. It is well known that the influence of small, close companions can produce secular alterations on the dynamics of the primary system (Athanassoula 1984; Sundelius et al. 1987; Byrd & Howard 1992). Moreover, the effects can manifest themselves on very different time scales. To cope with all those aspects, we define a galaxy as isolated when the possible past perturbations by neighboring objects, if any, have been completely erased by now. Accepting that typical time scales for the decay of the perturbation effects are not longer than a few times 10^9 years, a criterion as given before can be defined.

Given the incompleteness of the CfA catalog, and the lack of red-shift information for many of the possible companions, we have adopted the parameter f, defined as $f = 3 \times log(r/D) + 0.4 \times (m - m_p)$ [2] to describe the environmental status of our sample galaxies. Numerical results (Athanassoula 1984) indicate that ponderable effects are expected for f larger than -2. To take into account the possible past effects, we have adopted as truly isolated those galaxies with $f \leq -4$ (the details and justification of the adopted criterion will be given in Varela et al., in preparation). The search for companions was done with a catalog complete to $m_B = 18$, kindly made available to us by G. Paturel. The results were visually inspected to discard any candidate that is not a galaxy. As a result, we have an indication of the status of each galaxy just given by the maximum of the f values corresponding to all its (candidate) companions.

According to that status we have classified our sample galaxies into 3 groups. The first one includes 24 truly isolated galaxies in the sense defined before (interaction class INT = 1); the second, with 44 objects, includes possibly interacting galaxies, with a companion (with log f > -4) of unknown red-shift (INT = 2); it will most probably contain both truly isolated and truly interacting galaxies and will therefore be considered separately from the others. Group 3, with 43 objects, is for interacting galaxies, including the 22 galaxies in Karachentsev's pairs and the 21 isolated spirals from the authomatic rearch that resulted to have confirmed companion(s). The type and absolute magnitude distributions of the two subgroups included in the last Interaction Grop are similar. We have performed the Kolmogorov-Smirnov test and found that they are not significantly different, and therefore can be considered as defining the same group.

2.2. Characterization of the sample

We have considered the morphology and luminosity of the whole sample galaxies to see if the selection criteria would have resulted in differences among the galaxies with different status. The type and magnitude are from the RC3 catalogue. The distribution of the types is shown in Fig. 1a. It appears that 37 galaxies have t < 4, and 47 have $4 \leq$ t < 6). The remaining 27 galaxies with t ≥ 6 (24%) (12 galaxies with t = 6) present different morphological peculiarities, but in all cases an underlying disk does exist.

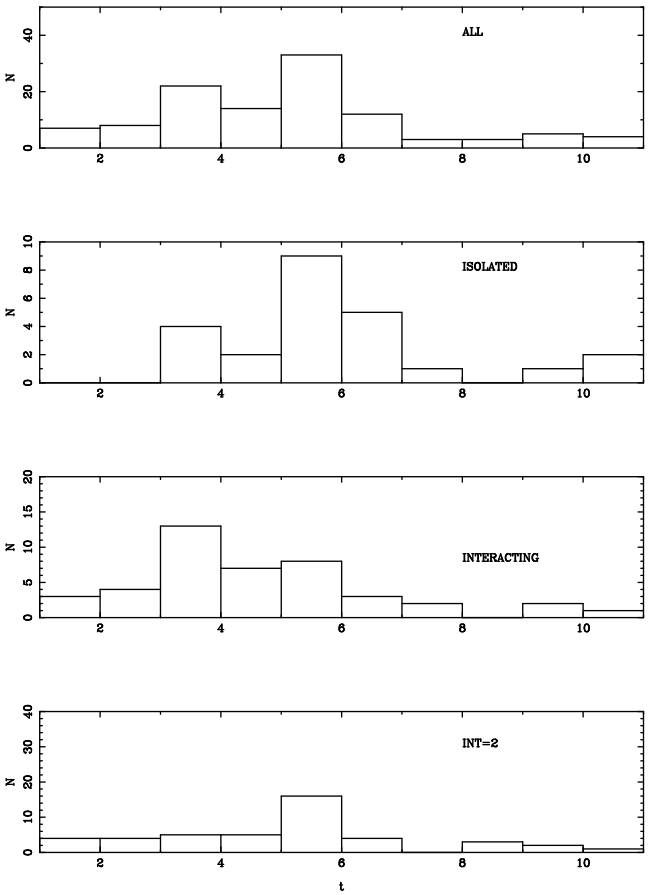

Fig. 1. Distribution of morphological types in our sample.

We have compared the morphology of the confirmed isolated galaxies (Interacting Type 1, 24 objects) with that of interacting galaxies (Interacting Type 3, 43 objects). As can be seen in Fig. 1, both t-distributions look different, in particular due to the lack of galaxies with t < 3, plus the scarcity of t = 3 galaxies (only 4) among the isolated objects in our sample. To quantify the differences we performed a Kolmogorov-Smirnov test, finding that, at the 95% level, the difference is statistically significant. The same kind of result is found when only galaxies with t $<$ 7 are considered.

Regarding the presence of bars for the whole sample, 32 are barred systems (SB code in the RC3), 24 are of intermediate type (SX), and 34 have been classified as unbarred systems (SA). We notice that these numbers are similar to those reported in studies on the fraction of barred spirals based on optical studies (see for instance Moles et al. 1995; Ho et al. 1997). For the other 21 galaxies there is no information about the presence of a bar in

[2] D is the distance from the target galaxy to the perturber, r is the radius of the target galaxy, m is the magnitude of the target galaxy and m_p is the magnitude of the perturber.

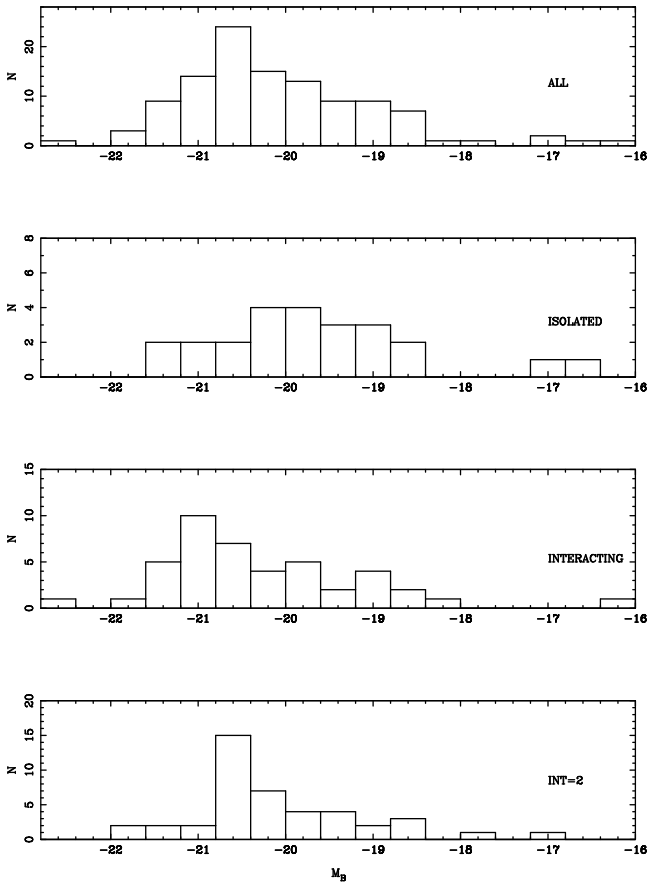

Fig. 2. Distribution of B absolute magnitudes.

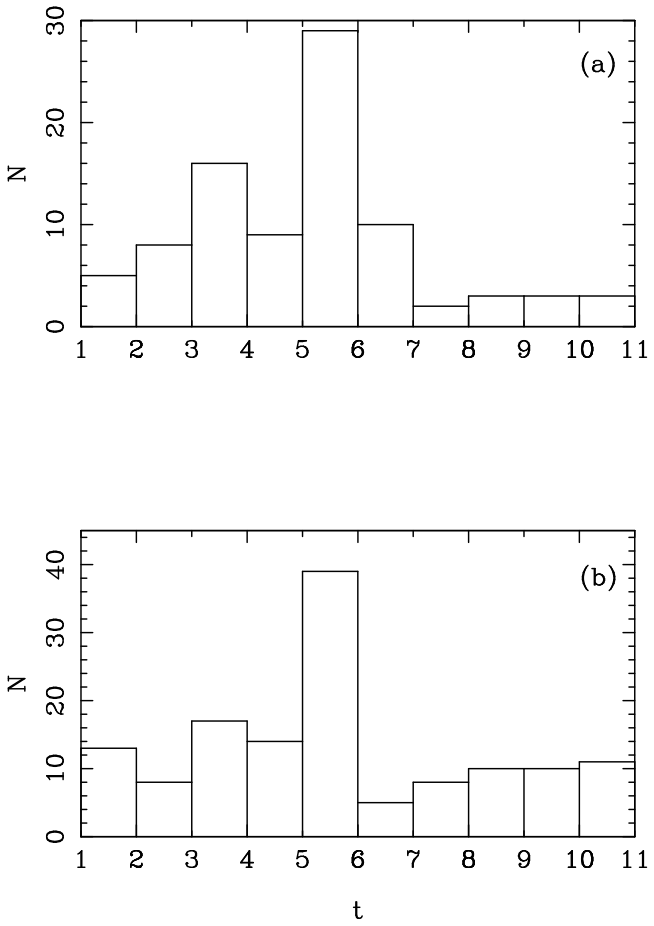

Fig. 3. Comparison of the distribution of morphological types for authomatically selected isolated galaxies in our sample (a) and in Jansen's sample (b).

the RC3. The same percentage of isolated objects (33%) is found among barred and unbarred galaxies.

The distribution of absolute magnitudes for the whole sample is given in Fig. 2. The absolute magnitude ranges from -16.31 to -22.43, the low luminosity tail corresponding to late type galaxies with morphological classification later than t = 6. For those late types alone, the median value is -18.63, whereas it reaches -20.42 for the other types. Looking at those galaxies with t $\leq$ 6, we find that the interacting objects tend to be brighter, $M_B = -20.69$ mag, *versus* $M_B = -20.28$ mag for isolated objects, with a dispersion of 0.62 mag in both cases.

Both the morphological type and absolute magnitude distributions for the whole sample are similar to those of the spiral galaxies analyzed by de Jong & van der Kruit (1994), who also selected non-disrupted spiral galaxies. We have also compared with the sample by Jansen et al. (2000): considering galaxies defined as isolated with our first criteria, i. e., with no companions within a projected distance of 0.5 Mpc, or with a red-shift difference greater than 500 km/s, the t-distribution is similar to that of our galaxies, excepting that their selection method produces more t$\geq$7 galaxies and (by construction) a much flatter distribution of absolute magnitudes (see Fig. 3). Indeed, the Kolmogorov-Smirnov test for galaxies earlier than t = 7 (92 and 79 galaxies in Jansen et al. sample and in our sample, respectively) gives the result that both distributions are not statistically different. We also note that only one galaxy among the 8 secondary members of the isolated pairs has t=3, the rest been later types. Therefore, we are confident that our sample galaxies is representative of normal spirals and it is not biased to any particular property, and the differences between isolated and interacting galaxies seem to be real.

3. Observations and Data Reductions

The spectroscopic data were collected with three different instruments: the Cassegrain Spectrograph attached to the 2.2m telescope in Calar Alto (CAHA, Spain), the Intermediate Dispersion Spectrograph at the 2.5m Isaac Newton telescope in La Palma (Spain), and the Boller & Chivens spectrograph attached to the 1.82m Asiago-Ekar telescope at the Asiago Observatory (Italy). The setup and main characteristics of the observations are given in Table 1.

All the galaxies were observed with the slit oriented along the galaxy major axis. We determined the PA of the axis from our own broad band images (Paper I), or from DSS images. In most cases the values we measured are very close to that catalogued in the RC3. In general the

differences are within 15°. Only in three cases we found a big discrepancy, namely for N3769a (40°), N3044 (100°), and U11577 (85°). In those cases we adopted our own values for the PA of the major axis. The PA are given in Table 2, together with the exposure time. For 22 galaxies we also obtained spectra along one additional PA, corresponding in 16 cases to the minor axis.

The data obtained in Calar Alto and La Palma were reduced in a similar way, using the appropriate routines in FIGARO. After bias subtraction, and flat field correction, the data were wavelength calibrated using He-Ar comparison spectra, that were observed before and after each object exposure. The resulting accuracy was tested using the sky lines [OI]λ6300, and [OI]λ6364, as references. The centroids of the lines were measured section by section. The average value was then compared with the reference wavelengths to fix the zero-point offset of each spectrum, and the rms error as an indication of the error in the resulting velocity distribution induced by the residual distortion (see Table 2).

The sky background level was determined taking median averages over two strips at both sides of the galaxy signal. The parameters of the lines were measured with the program LINES kindly provided to us by Dr. Perea. This program perform a simultaneous interactive polynomial fitting of the continuum and Gaussian fitting of the emission selected lines providing the Equivalent Width, central wavelength of the Gaussian fit and the integrated fluxes of the lines. The errors in Table 5 have been calculated by quadratic addition of photon counting errors and the errors in the continuum level determination.

We used cross-correlation technics as described in paper I to extract the kinematic information. The spatial section in the 2D spectrum with the highest S/N ratio was used as a template for the cross-correlation. The errors are referred to the determination of the velocity shift with respect to the template spectrum. They are shown as the error bars in all the velocity distributions (see Figs. 4 and 5).

The data obtained at Asiago (a total of 29 galaxies) was reduced using IRAF routines, with the same criteria and definitions as for the other data.

4. The shape of the rotation curves

The long slit spectra along the major axis we obtained contain adequate information to elaborate the rotation curves for 78 out of the 85 galaxies. They are presented in Figs. 4 and 5. The 7 galaxies with velocity distributions not reliable enough to trace their rotation curves are NGC 3507, NGC 5394, NGC 5641, NGC 2344, NGC 1036, NGC 5375 and UGC 11577. The parameters derived from our rotation curves (without further correction) are given in Tables 3 and 4.

The kinematic center was defined as that section for which the differences between the two branches of the rotation curve (in particular, for the most symmetric region which normally corresponds to the central parts), are minimized. In most cases, within our resolution, that center corresponds to the photometric center, i.e., the absolute maximum in the continuum distribution along the slit. The red-shift corresponding to that kinematical center was adopted as the red-shift of the system in all cases and is given in Tables 3 and 4. The derived distances were determined allowing for correction for galactocentric motion, following the RC2, and for virgocentric motion. Since the galaxies are rather nearby, the last correction should be considered. It was calculated following Kraan-Korteweg (1986; model 1). We found that those corrections typically amount to less than 15%. The distances calculated from the corrected values and $H_0 = 75$km s^{-1} Mpc^{-1} are given in Tables 3 and 4.

We have also obtained 21 additional spectra, 16 of them along the minor axis. The resulting velocity distributions are shown in Figs. 6 and 7. We notice that for NGC 2543 and NGC 5963 the velocity distributions along the quoted minor axes show velocity amplitudes for the outskirts of about 50 km/s, implying that a misalignment exists between photometric and kinematical minor axes. For NGC 7217 and NGC 7479 the resulting amplitude is much higher, up to about 100 km/s. The presence of non-circular motions is clearly detected in the central regions of NGC 1530, NGC 2543, NGC 5351, NGC 5480, NGC 5656, NGC 5963, NGC 7177, NGC 7217 and NGC 7479. We note that, excepting NGC 5656 and NGC 5963, for which the detailed morphological classification is missing in the RC3 catalogue, the other galaxies are classified as having rings, and four of them are weakly (NGC 7177) or strongly (NGC 1530, NGC 2543, NGC 7479) barred. Non-circular motions are detectable in 3 out of the 5 non-major-axis spectra, namely NGC 5394, NGC 5899 and NGC 2906, in the inner 5, 10 and 7 arc-seconds, respectively. The exact connection between morphological and kinematical features, for which the imaging is needed, is out the scope of this paper. We just note that the percentage of galaxies showing noncircular motions (11%) is in agreement with the 17% reported by Rubin et al. (1997).

Different parameters are used to describe the rotation curves depending on their final purpose. We have measured all the parameters that could be of some interest for statistical purposes. In particular we have measured the first local maximum, V_{max}, in the observed velocity distribution, and the corresponding distance to the center, R_{max}. We have also measured the slope, G (in km/s/Kpc) of the inner rotation curve. This parameter, directly related to the bulge-to-disk ratio, appears as one of the two main parameters (together with the total mass or luminosity) to describe the family of isolated spiral galaxies and correlates with the bulge-to-disk ratio better than the morphological type (Paper I and II and see below). Indeed, we also measured the absolute maximum velocity, V_m, and the central distance at which it is reached, R_m, and the maximum extent of the observed rotation curve, R_M. All those parameters show relations between them and with other galactic properties. Thus, as shown in Fig. 8, later type galaxies tend to have lower G values (see also

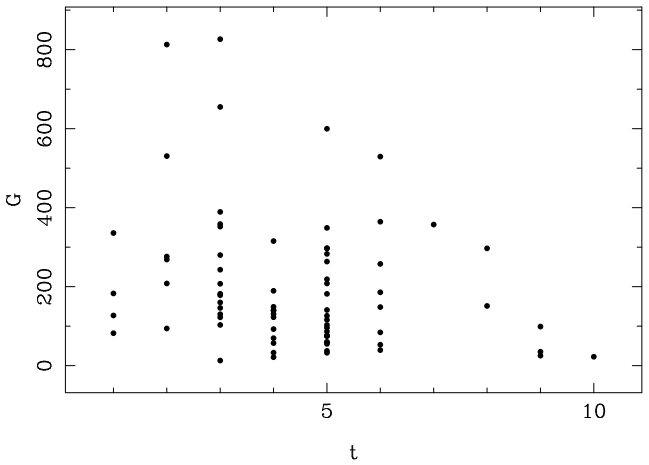

Fig. 8. Distribution of G values (representing the inner solid-body rotation gradient) as a function of the morphological type, t.

Paper II and Baiesi-Pillastrini 1987). A better correlation was found between the same slope G, and a quantitative descriptor of the morphological type as the bulge to disk ratio, B/D, in particular for isolated galaxies (Paper II). Unfortunately, the available photometric data in the literature is not abundant and homogeneous enough to further test that relation here.

Regarding the outer part of the rotation curve, a descriptor was defined (Paper I and II) for its behavior,

$$\Delta = arctan[((v_m - v_{max})/max(v_m, v_{max})) \times (r_m - r_{max})/r_{25}]$$

It takes values around zero for flat rotation curves, whereas it is positive for rising curves and negative for declining curves. The distribution of this parameter for isolated and interacting is shown in Fig.9. We find that for isolated galaxies $\Delta = 0 \pm 7$, and for interacting galaxies $\Delta = 5 \pm 16$. This result confirms and extends the earlier one reported in Paper II, where galaxies in isolated pairs were compared to isolated galaxies.

Sometimes a different parameter is adopted to describe the gradient of the outer rotation curve, defined as (see for instance Dale et al. 2001),

$$OG = [V(0.70 \times R_{25}) - V(0.35 \times R_{25})]/V(0.70 \times R_{25})$$

We found OG = 7.8±6.6 for isolated galaxies and 10.4±15.5 for interacting galaxies, showing that both parameters, Δ and OG give similar information about the outer rotation curve.

Regarding the maximum velocity[3], V_m, it has been known that it is also related with the morphological type (Rubin et al. 1991). We find the same tendency with the present data set (Fig. 10). The median values for type 1 to 6 are 223±46, 253±29, 194±41, 160±33, 186±37, and 142±37, respectively. The same V_m is related to the absolute magnitude (Fig. 11), with less scatter for the isolated objects.

[3] All the velocities have been corrected for inclination following Peterson et al. (1978).

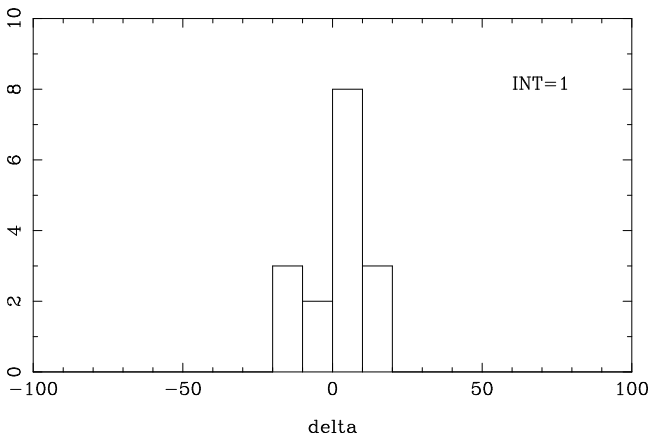

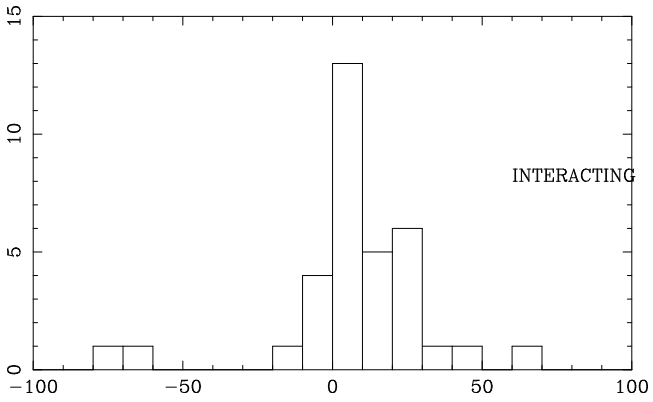

Fig. 9. Distribution of Δ values (representing the shape of the outer rotation curve.

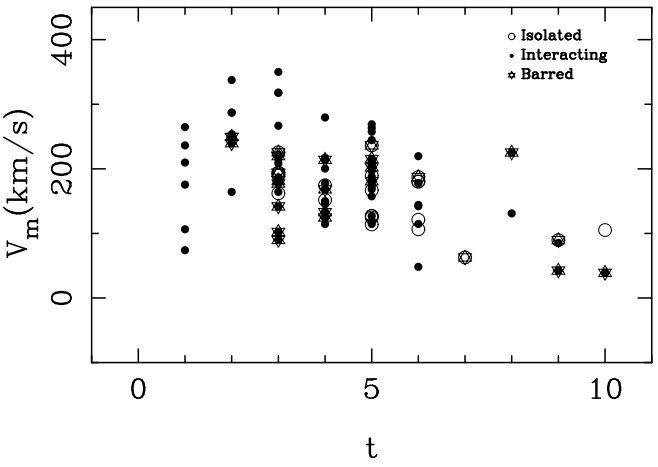

Fig. 10. Absolute maximum velocity versus morphological type, t.

We have further investigated whether there the tendency found by Rubin et al. (1999) for later spiral galaxies to show more extended HII distributions, what translates into longer rotation curves. This tendency is confirmed, as shown in Fig. 12, where the maximum extension of the rotation curve, R_M (in units of R_{25}) is plotted versus the morphological type. The increasing trend is clear for spi-

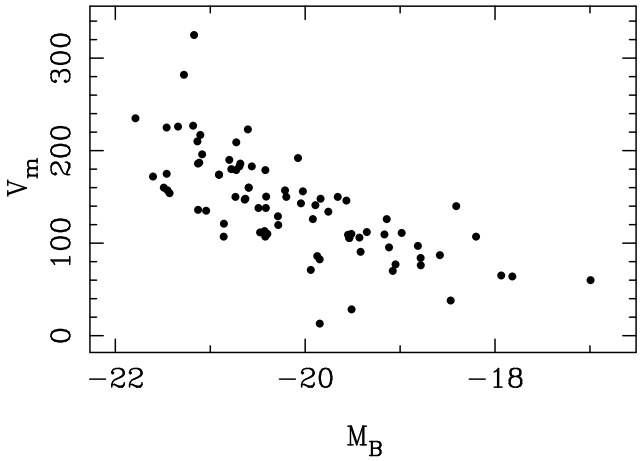

Fig. 11. Absolute maximum velocity as a function of absolute B magnitude.

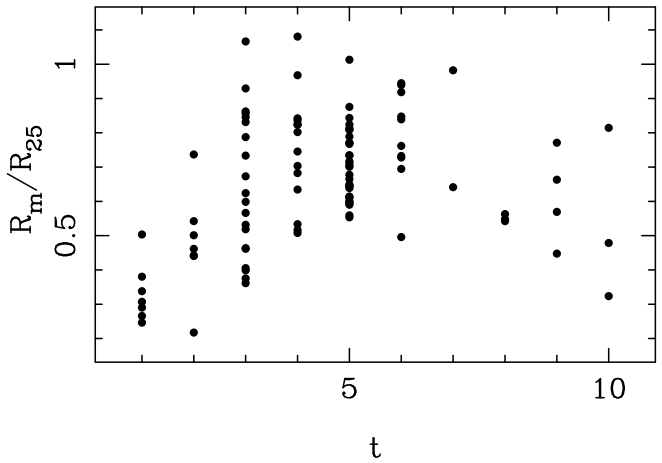

Fig. 12. Maximum extension of the rotation curve, R_M (in units of R_{25} *versus* the morphological type t.

rals up to t = 6. No difference is found when the sample is separated according to the interaction state.

The central mass (inside the solid-body rotation region) seems to be slightly higher for early type galaxies, consistent with them hosting bigger bulges. No tendency is found between central mass and interaction class. The total masses within R_M and R_{25} (this last from the RC3 catalogue), for an homogeneous and spherically symmetric distribution ($M_T = 2.3265 \times 10^5$ r v^2(r) $M_\odot$, with r in Kpc and v(r) in km/s) are also given. The M/L relation is similar for galaxies with t<7, with no clear trend neither with the morphological type, nor with the interaction class.

5. The Tully-Fisher relation

As shown by Courteau (1997), the best kinematical tracer is $V_{2.2}$, which is the velocity attained at $R_{2.2} \approx 2.2\ r_d$ (r_d = disk scale length). Instead of r_d we have used $1.3\times R_{eff}$, equivalent to $0.65\times R_{25}$, that results to be a good approximation for spiral galaxies and does not require a bulge-disk decomposition (Courteau 1997). Since the rotation curves derived from optical emission lines do not usually reach $R_{2.2}$, we fitted a model curve to the observed rotation curve in the inner part of the galaxy, and extrapolate it to the outermost regions. We have followed that procedure using models as simple as possible. We have used the normalized arctangent rotation curve fitting function given by

$$v(R) = v_0 + 2/\Pi \times v_c \times arctan(R)$$

with $R = (r - r_0)/r_t$, v_0 is the velocity center of rotation, r_0 is the spatial center of the galaxy, v_c is an asymptotic velocity and r_t is a radius that corresponds to the transition region between the rising and the flat parts of the rotation curve. This function has been shown to reproduce adequately the shape of the rotation curves with the smallest number of arguments (Courteau 1997) and emerges naturally from the standard parameterization of the density profiles of dark halos (Gilmore et al. 1990). As noted by Courteau (1997) the resulting parameters cannot be used to describe rotation amplitudes and scales, but since it allows to trace smoother curves and to somewhat extrapolate to $0.65\times R_{25}$, it will be useful for our purposes. The model curves are shown in Figs. 4 and 5. According to this model, we have calculated the residuals, what allows us to obtain a quantitative estimation of the the goodness of the model: the rotation curves are classed as regular when the differences between the observed and the arctangent velocity distributions are smaller then 10%; if these differences are higher than 10% but the shape of the curve still follows that of the model, the curve is classified as distorted; the rest are considered as peculiar. The curves may be also symmetric or asymmetric in the extension of the two branches. Therefore, the final classification is as following: 1: regular and symmetric; 2: regular and asymmetric; 3: distorted symmetric; 4: distorted asymmetric; 5: peculiar.

The resulting TF relation is shown in Fig. 13, where the different interaction classes have been marked with different symbols. It can be seen that isolated galaxies trace the TF relation with the smallest scatter. Moreover, the three outliers belong to the group of interacting pairs. We have quantified the residuals with respect to the TF relation as given by Tully & Pierce (2000). We find 0.32 for isolated galaxies (INT = 1) and 0.65 for interacting spirals (INT = 3). We notice that the three outliers (NGC 2799, NGC 3395 and NGC 3396) show peculiar rotation curves (only NGC 2799 is not later than t = 6, but is a secondary member), and that their position is much closer to the TF line when HI velocity amplitudes are considered. The same analysis has been applied to isolated and interacting objects. Therefore, even if the results shown here are only indicative due to small number statistics, we point out that a possibility seems to exist for reducing the scatter of the TF relation determined with optical data when using the most isolated objects.

We have also explored the eventual dependence of the departures from the TF line as a function of the degree

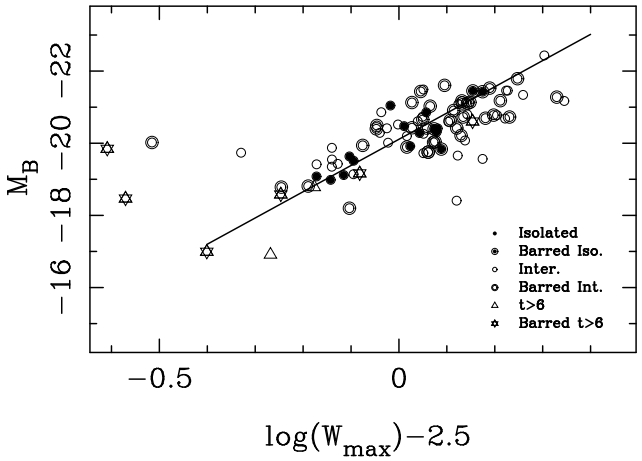

Fig. 13. TF relation for our sample galaxies. The solid line represents the TF line by Tully & Pierce (2001).

of peculiarity of the rotation curves.[4] The dispersion from the canonic TF line is 0.30 for galaxies with regular rotation curves, 0.34 for galaxies with distorted rotation curves and 0.36 for peculiar rotation curves. This appears to be at variance with the results reported by Barton et al. (2001) who found that the presence of strong kinematic distortions is a significant predictor of TF residuals. The difference could be due to the fact that, as already pointed out, our sample includes only isolated and mildly interacting objects, that do not present strong distortions. Our data are in agreement with Dale et al. (2001) who find no differences between cluster and field spirals in the degree of asymmetry.

6. Nuclear and Disk spectral characteristics

The distribution of the Hα line emission along the slit was traced for each 2D spectrum. The local peaks in the distribution were taken as the centers of HII regions, that were defined to comprise all the spatial sections within the FWHM around that peak. The resulting 1D spectra were measured as explained before, producing the data collected in Table 5. In the following the region comprising the center of the galaxy is referred as the Nuclear Region. Typical sizes for the Nuclear Regions range between 0.5 and 2 kpc. The spectra are not flux-calibrated. However, since the lines used in the analysis are very close in wavelength, the count ratios are a good measure of the flux ratios.

Given the spectral coverage of the data, the standard diagnostic tools to classify the spectra (Baldwin et al. 1981, Veilleux & Osterbrock 1987) cannot be used. But, as shown by the early work by Keel (1984), the [NII]/Hα line ratio can be used as a rough, first order estimator to classify the spectral nuclear types (SNT) into Active Galactic Nuclei (regardless of the kind of activity, since into the AGN category we have included both Seyfert and LINER-like nuclei) and HII like objects. Accumulated evidence has shown that that line ratio is very sensitive to the presence of any kind of activity, thus allowing for an easy spectral classification of the nuclei. The existence of absorption under the Balmer line could however induce the misclassification of some objects, and special care has to be taken.

Apart from a spectroscopic classification of the nuclear spectra, we have also attempted to give an estimation of the metallicity of the disk and its possible gradient, taking the [NII]/Hα line ratio as an estimator. For low metallicity objects both, Nitrogen and Oxygen are of primary origin and their abundances correlate well (Masegosa et al. 1994). For higher metallicities, a fraction of the measured Nitrogen is of secondary origin, what modifies the previous relation, even if it is still monotonic and, therefore, useful to probe Z. van Zee et al. (1998) have found that, for $12 + \log(\mathrm{O/H}) < 9.1$, a relation does exist of the form $12 + \log(\mathrm{O/H}) = 1.02 \log([\mathrm{NII}]/\mathrm{H}\alpha) + 9.36$. The use of the [NII]/H$\alpha$ line ratio to estimate Z has the advantage of being insensitive to reddening. But, as Stasinska & Sodré (2001) have pointed out, that calibration relation is adequate only for HII regions, and important errors could be produced when the integrated spectra of spiral galaxies, or a complex ISM with shocked gas is being analyzed. Based on the [NII]/Hα ratio Denicoló et al. (2002) obtained an improved calibration on the oxygen abundances. They clearly showed the power of this estimator when analyzing large survey data to rank their metallicities, even if the uncertainties on individual objects can reach up to 0.6 dex, mainly due to O/N abundance ratio and ionization degree variations. Here we only consider it to study global trends of Z from the spectra of HII regions or HII-like nuclei in the collected sample of spiral galaxies.

6.1. Nuclear spectra

Nuclear Hα emission has been detected in 91 out of 98 galaxies in the sample. For the other 13, the stored data were corrupted. The nuclear spectra are presented in Fig. 21. Three of the galaxies without Hα emission (namely, NGC 3976, NGC 5641, and NGC 2424) show [NII] emission, suggesting that shock ionization would be important in these nuclei. They were classified as LINERs in previous studies (Carrillo et al. 1999), and they belong to the class of interacting systems. For the remaining 4 galaxies (NGC 2344, NGC 2545, NGC 3835 and NGC 5147) only very faint or even absent emission has been detected partly due to the poor S/N ratio of the spectra. In any case the emission cannot be strong. They do not show any other peculiarity and can be considered as normal spiral galaxies (Jansen et al. 2000).

Given the purpose of the work and the rather low S/N ratio in many of the spectra we have not applied any cor-

[4] Notice that systematic effects in the third parameter analysis cannot not be addressed mainly due to the lack of accurate enough photometric information in our sample galaxies (see Kannappan et al. 2002).

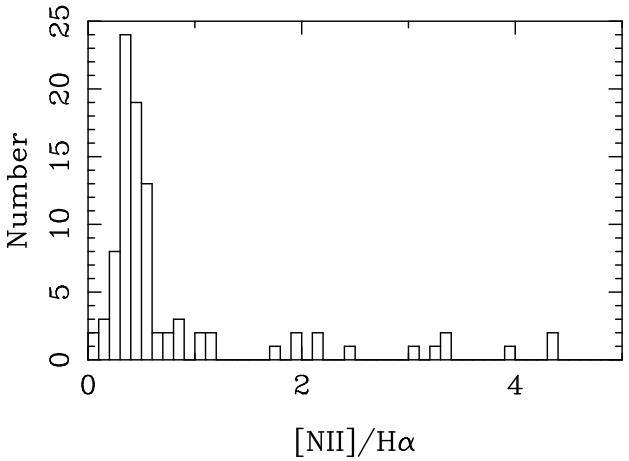

Fig. 14. Distribution of nuclear [NII]/Hα for the whole sample. NGC 7217 has not been included due to the large measured ratio (see text).

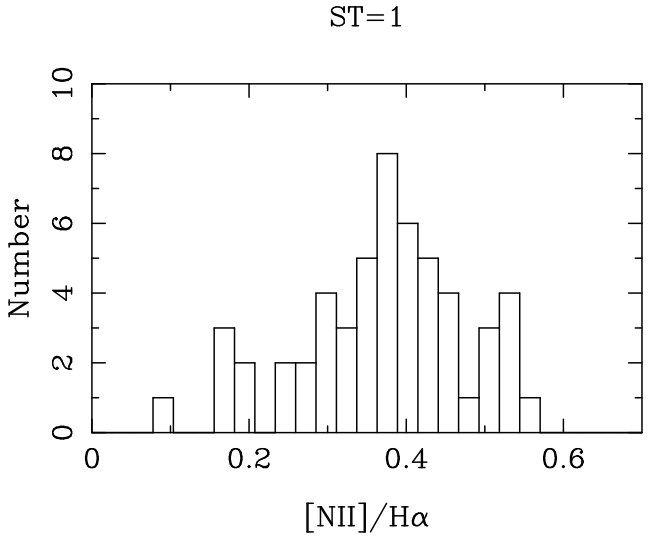

Fig. 15. Distribution of nuclear [NII]/Hα for the galaxies with nuclear spectral type SNT = 1.

rection for absorption. To cope with the problem of the presence of absorption under Hα, we visually inspected all the spectra, identifying the cases where it was conspicuous. All those galaxies were classified as SNT = 3, i. e., nuclei in which the Balmer absorption is so strong that the measured [NII]/Hα ratio is not reliable to classify it. For the remaining nuclei, without any appreciable absorption under Hα, those with spectral characteristics of HII regions were classified as SNT = 1, and those with line ratios similar to active galaxies as SNT = 2. Indeed this is a rather crude classification but, as we will see later, some conclusions on the nuclei of spiral galaxies and their relation to some global properties can be drawn.

The distribution of the [NII]/Hα nuclear values shows that for most of the galaxies it is lower than 1 (see Fig. 14). The data are presented in Table 5. We notice that all the galaxies with SNT = 3 have EW(Hα)$\leq$ 10, what produces an artificially high ratio if no correction is applied to cope with the underlying absorption and are consequently excluded hereafter from the discussion.

Judged from the [NII]/Hα ratio, we find 11 AGN candidate objects (about 10%) in our sample. Seven of them were already observed by Ho et al. (1997), who classified them as 6 LINERs and 1 Seyfert. For the remaining 4 galaxies we find that 2 of them are Seyfert 1 based on the width of the Hα line. For the other two the information we have is not enough to classify them as Seyfert 2 or LINER. The largest line ratio is found for N7217, with [NII]/Hα = 8.6. It is a known LINER (Filippenko & Sargent 1985) frequently quoted to illustrate the signature of strong shocks (see the models by Dopita & Sutherland 1995).

Regarding the HII-like nuclei, we find that they define a rather narrow distribution of the [NII]/Hα ratio (Fig. 15). Only two galaxies (not shown in the figure) depart from the general trend, N5172 with [NII]/Hα = 1.92, and N5678 with [NII]/Hα = 1.16. For N5172, our data are of very poor S/N ratio and the [NII]/Hα ratio we obtained is very uncertain. And N5678 is a composite LINER/HII galaxy after Filho et al. (2000). Excluding those two objects, the remaining galaxies present a range of values of the line ratio, corresponding to values typical of irregular galaxies and disk HII regions (see Vila-Costas & Edmunds 1993 and McCall et al. 1985). For all the data classified as SNT = 1, (with the quoted exceptions), included the latest spirals (t > 6), the median value is 0.38, with a dispersion of 0.07. Excluding late type spirals it amounts to 0.39 with the same dispersion.

In spite of the rough character of the estimator we use here, some correlations are already hinted. There is a relation between the metallicity of the HII-like nuclei and the morphological type, the early type spirals having more metallic nuclei than the later spirals (Fig. 16, and Table 6). This result is consistent with the suggestion by Oey & Kennicutt (1993) that early type spirals are more metal rich than later types. That results rests on the difference between Sa/Sab galaxies in one side, and the later types in the other, since we don't find any difference between Sb/Sbc and Sc/Scd objects. Indeed, the later than Scd types are still of lower Z and look as a different family. The results reported here are in agreement with the work by Zaritsky et al. (1994) based on a completely different data set, in the sense that a tendency does exist for the metallicity to decrease when moving along the Hubble sequence. We have investigated if such a trend could be due to a systematically stronger Hα absorption in early types. The absence of any appreciable trend between the Hα EW and the morphological type t argues against that explanation, and leaves the relation as genuine.

Finally, the analysis of a possible Z enhancement produced by the presence of instabilities like bars or by the interaction with nearby neighbors has produced negative results. The range and median value of Z does not seem to be altered when those aspects are taken into account.

We have shown in Paper II that the relations are better defined if the type is replaced by a more quantitative

Table 6. [NII]/Hα ratios for the three spectral nuclear types, and for the different morphological types.

	[NII]/Hα
SNT=1	0.38
SNT=2	0.98
SNT=3	0.76
t=1,2	0.46
t=3,4	0.38
t=5,6	0.38
t>6	0.27

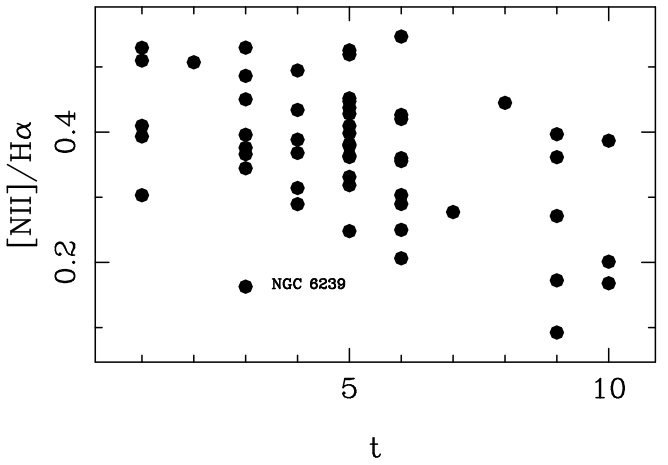

Fig. 16. [NII]/Hα ratios as a function of the morphological type.

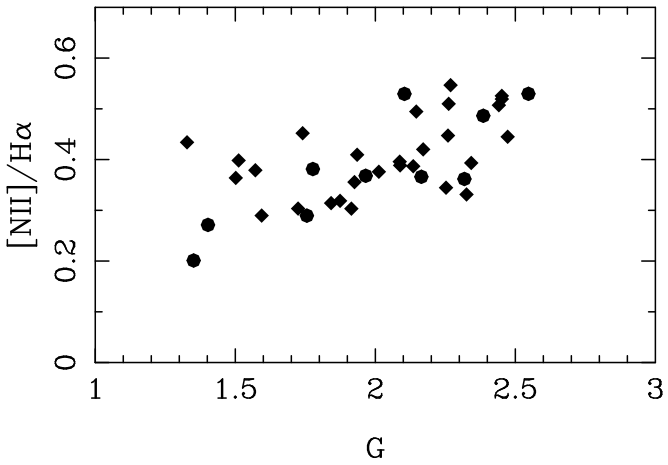

Fig. 17. Nuclear [NII]/Hα ratios as a function of the gradient of the solid-body region of the rotation curve, G. (G is in logarithmic scale). Interacting galaxies are marked with solid circles.

parameter such as B/D ratio, or the inner gradient G, with which it is tightly correlated. Here too, we find a good correlatin between Z and the gradient G (see Fig. 17), statistically significant at 99.99% confidence level (R = 0.63, for 38 objects). This add to the previous findings about the quality of the parameter G to characterize the global properties of spiral galaxies.

The other two global properties which appear to be related to the metallicity are the absolute magnitude, M_B and the maximum rotation velocity. We find that Z increases with both, the central velocity and the luminosity, i.e, massive galaxies are more metal rich. This agrees with the results reported by Zaritsky et al. (1994) and by Dutil & Roy (1999). Again no difference is found between isolated and interacting galaxies. These results would suggest that the instabilities produced by gravitational interaction, even if they can drive gas to the center (Barnes & Hernquist 1991; Mihos et al.), do not have major effects in the central region for mild interaction as the ones reported in this work.

6.2. Extranuclear HII regions

The extranuclear HII regions detected in all our 2D spectra were measured and used to characterize the metallicity of the disks. As discussed before, our data does not allow to conclude on any individual galaxy, but can be used to look for general trends when the population of the disks is considered as a whole. To be able to combine data from different galaxies, we have normalized to R_{25} (as given in the RC3) the galactocentric distances of the HII regions. In principle the choice of one or another radius to normalize could have some effect on the results about Z gradients (Zaritsky et al. 1994). Since we are interested on general trends and not in a real quantification of the gradient we consider that the choice of the normalization is of minor importance and decided to use the isophotal radius, accessible for most of the galaxies studied. From the HII regions measured we have only selected all the data with Hα equivalent width larger than 10 Å. In that way we select the better S/N data, and avoid including regions with important Balmer absorption, that could induce inconsistencies in the estimation of the metallicity. The number of regions we consider here is 392, in 98 galaxies. In the following we report the results obtained when the general metallicity trends in the disk are analyzed in relation to the morphology of the galaxy, the Nuclear Spectral Type and the effects produced by interaction. Different authors have claimed (see Vila Costas & Edmunds 1992 for a review and Zaritsky et al. 1994) that a Z radial gradient does exist in disk like galaxies. In Fig. 18 the metallicity estimator [NII]/Hα is presented for the different morphological types. A slight tendency seems to be present for the gradient to be steeper in later types, whereas it is about zero for Sa and Sb spirals. This agrees with the claim by Oey & Kennicutt (1993) of a larger global metallicity and almost flat gradients in early type spirals.

We have calculated from the disk data the expected central [NII]/Hα values, using the formal fitting to the data. The values we find in that way ranges from 0.41 for the earlier types, to 0.28 for the latest types. They compare very well with what we have found just measuring the line ratio of the nuclear regions, 0.44 for the early types, and 0.27 for the latest types. That consistency adds confidence to the reality of the trends we have found, and to the way of estimating the metallicity form the line ratio.

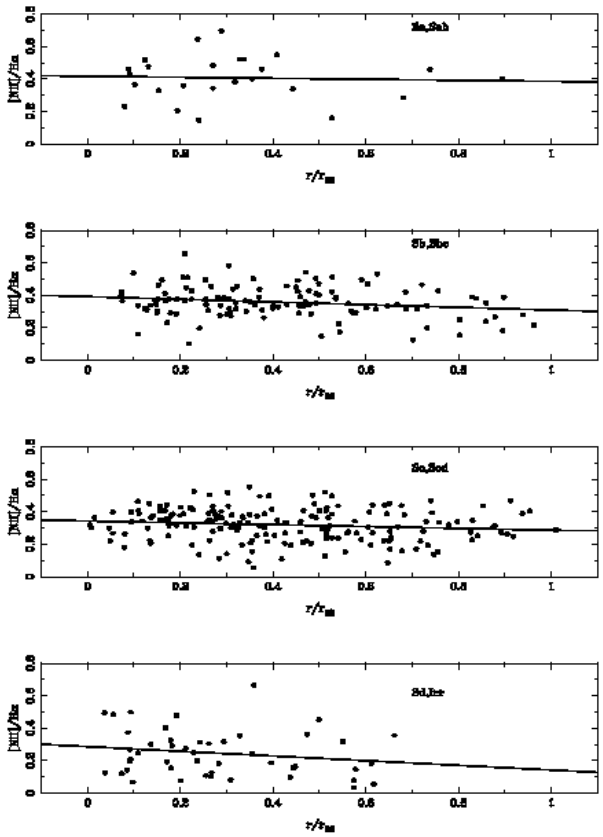

Fig. 18. Disk [NII]/Hα ratios as a function of the distance to the center (normalized to R_{25}).

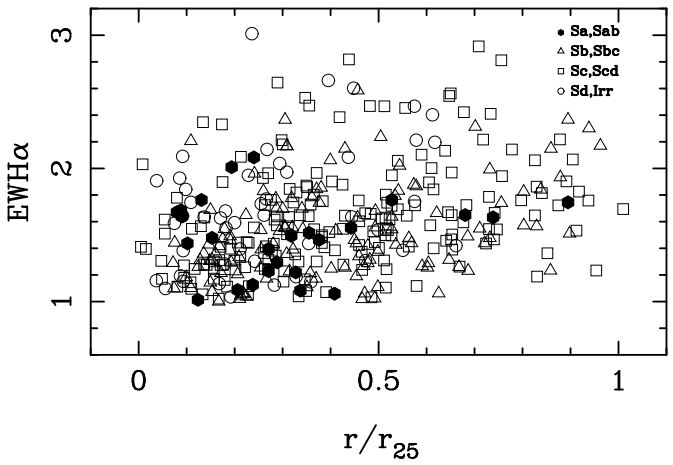

Fig. 19. Disk equivalent widths of Hα (in Å) as a function of the morphological type, t. EWs are plotted in logarithmic scale.

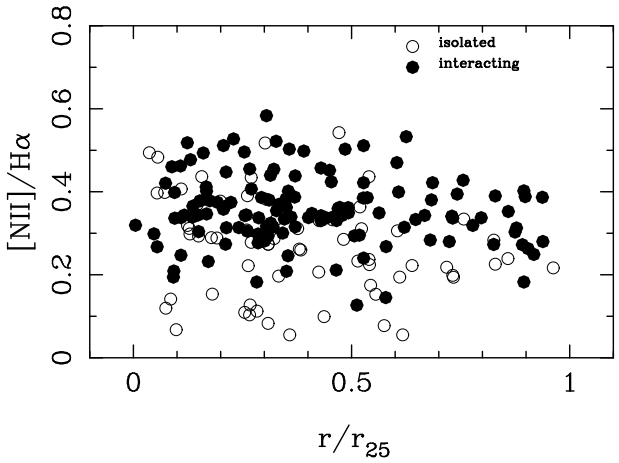

Fig. 20. Metallicity estimator for the HII regions in the disks of isolated and interacting spirals.

The Hα Balmer line has been extensively used to measure the ratio of the current to the average past Star Formation Rate in Galaxies (see Kennicutt 1983, Kennicutt et al. 1994, and Stasinska & Sodré 2001). Kennicutt (1994) found smooth progression in the Star Formation History with the Hubble type, with a ratio of current to past SFR increasing from 0.01-0.1 for Sa type to 0.5-2 for a typical Sc disk. The data reported here are only barely consistent with such claim. In Fig. 19, where the Hα equivalent width is plotted versus the radial distance, the only effect is a larger dispersion on later types than in earlier spirals towards larger EW in the later types but a clear separation between different morphologies is not obvious. It has to be noticed that Kennicutt data are referred to the integrated EW whereas here we are trying to get the trend based on the distribution of HII regions crossed by the slit through the disk of the galaxies. We cannot extract a definitive conclusion from our data and, therefore, we cannot say that our data are in contradiction with Kennicutt's study, even if such a conclusion is hinted by our results.

Let's now compare isolated and interacting systems. Regarding the metallicity, it appears that interacting galaxies tend to show a larger [NII]/Hα ratio in all the mapped regions (see Fig. 20). The median value of [NII]/Hα for the disk of isolated normal galaxies amount to 0.27, in contrast with a median value of 0.35 for the interacting systems.

It is usually accepted that the interaction process drives gas to the central regions producing an enhancement in the star formation events. Consequently, a larger Z in the bulges of those galaxies would be predicted, and it's found in our data and other studies. The point here is that we have also found a higher Z along the disks of the same galaxies. It seems then that the interaction affects the whole galaxy, producing star formation in all the disk, depending on the conditions (see for example, Márquez & Moles 1994).

However, no difference in the Hα EW has been found between interacting and isolated galaxies, as if the global star formation rate now was essentially the same in both families. To understand this result we have to take into account that only mildly interacting systems are included in our sample, for which the effects of the interaction are expected to be much less important than in stronger interactions. In that sense, we notice that our results are

compatible with those found by Kennicutt et al. (1987) for a large fraction of galaxies in their complete pairs sample. Combining both results, higher Z and normal present star formation rate, it seems that the enrichment is only produced as a secular, accumulative effect along the galaxy life, without marked episodes, in those mildly interacting systems. This result is consistent with those by Bergvall et al. (2001), who find reddest disks in interacting galaxies. Nevertheless, we have already noticed that the morphological types of interacting galaxies tend to be earlier than for isolated ones, so the reported higher metallicities could be reflecting the difference in metallicities between early and late type galaxies. Larger samples of isolated galaxies would be needed to further analyze the metallicities of early types spirals as compared to those of interacting spirals with the same morphologies.

The situation for AGNs is somewhat similar, since active spirals are known to mainly reside in early types spirals (see for instance Moles et al. 1995). Given the limited sample we are considering (11 AGNs, 7 of them belonging to interacting systems) eventual differences in metallicity cannot be addressed.

7. Summary and conclusions

We have obtained long slit spectra along the major axes of a sample of spiral galaxies selected to be either isolated or in isolated pairs, with similar intermediate-scale environment and with a recognizable and well defined spiral morphology. We have further investigated their environmental status and reclassified them, what allows us to define a sample of isolated objects, to be later compared with mildly interacting spirals (with small satellites and/or companions of similar size). The main results we have obtained are the following:

- We have confirmed previous results (Paper II) that isolated galaxies tend to be of later Hubble types and lower luminosity than the interacting galaxies
- The outer parts of the rotation curves of isolated galaxies tend to be flatter than in interacting galaxies. They show similar relations between global parameters. The scatter of the Tully-Fisher relation defined by isolated galaxies appears to be significantly lower than that of interacting galaxies
- There is a clear trend between the metallicity of the HII-like nuclei and the morphological type of the galaxy, the earlier types showing larger Z values. Extrapolation of the Z-trend in the disk to the central position gives consistent results with the direct measurement of the nuclear HII region. No trend with the interaction status was found
- We report here for the first time the existence of a tight correlation between Z and the gradient of the inner rigid solid rotation part of the rotation curve, G
- The Z-gradient of the disks depends on the type, being almost flat for early spirals, and increasing for later types
- [NII]/Hα ratios appear to be larger for disk HII regions interacting galaxies. This could be simply due to the fact that early types are more frequent among them. (A similar result is obtained for AGNs, but we cannot further test it given the small size of our sample). On the other hand, the Hα EW present similar values in all kind of galaxies. At face value those results would indicate that mildly interacting galaxies (as those in our sample) have different histories form normal galaxies. This difference however has no marked episodes (bursts) of star formation, but only small cumulative effects that result in more metallic (and redder) disks and nuclei.

Acknowledgements. We are very grateful to the anonymous referee, whose comments and suggestions helped us improving the presentation. We thank Prof. G. Paturel who kindly made available to us prior to publication the Galaxy Catalog we have used to determine the interaction status of our sample galaxies. We also thank L. Cariggi for her careful reading of the manuscript and valuable comments. I. Márquez acknowledges financial support from the Spanish Ministerio de Ciencia y Tecnología and the IAA. D. Jesús Varela acknowledges a scholarship from the Ministerio de Ciencia y Tecnología. This work is financed by DGICyT grants PB93-0139, PB96-0921, PB98-0521, PB98-0684, ESP98-1351, AYA2001-2089 and the Junta de Andalucía. This research has made use of the NASA/IPAC extragalactic database (NED), which is operated by the Jet Propulsion Laboratory under contract with the National Aeronautics and Space Administration.

References

Athanassoula, E., 1984, Phys. Rep. 114, 319
Amram, P., Balkowski, C., Boulesteix, J. et al., 1996, A&A 310, 737
Baiesi-Pillastrini, G.C., 1987, A&A 1972, 375
Baldwin, J.A., Phillips, M.M., Terlevich, R., 1981, PASP 93, 5
Barnes J.E., Hernquist L.E., 1991, ApJ 370, 65
Barton, E., Geller, M.J., Kenyon, S.J., 2000, ApJ 530, 660
Barton, E., Geller, M.J., Bromley, B.C. et al., 2001, AJ 121, 625
Bergvall, N., Laurikainen, E., Aalto, S., 2001, A&A, submitted
Byrd, G.G., Howard, S., 1992, AJ 103, 1089
Carrillo, R., Masegosa, J., Dultzin-Hacyan, D., Ordoñez, R., 1999, Rev. Mex. A&A 35, 187
Conselice C.J., Gallagher, J.S.,III, 1999, AJ 117, 75
Conselice, C. J., Bershady, M. A., Jangren, A., 2000, ApJ 529, 886
Courteau, S., 1997, AJ 114, 2402
Dale, D.A., Giovanelli, R., Haynes, M. et al., 2001, AJ 121, 1886
Denicoló, G., Terlevich, R., Terlevich, E., 2002, MNRAS 330, 69
Dopita, M. A., Sutherland, R. S., 1995, ApJ 455, 468
Dutil, Y., Roy, J.-R., 1999, ApJ 516, 62

Filho, M.E., Barthel, P.D., Ho, L.C., 2000, ApJS 129, 93
Filippenko, A.V., Sargent, W.L.W. 1985, ApJS 57, 503
Ferguson, A.M.N., Gallagher, J.S., Wyse, R.F.G., 1998, AJ, 116, 673
Gilmore, G.F., King, I.R., van der Kruit, P.C., 1990, The Milky Way as a Galaxy, edited by R. Buser and I.R. King (University Science Books, CA), p. 212
Henry, R.B.C., Worthey, G., 1999, PASP 111, 919
Ho, L.C., Filippenko, A.V., Sargent, W.L.W., 1997, ApJS 112,315
Huchra, J.P., Vogeley, M.S., Geller, M.J., 1999, The CfA2s catalog, VizieR On-line Data Catalog: J/ApJS/121/287.
Jansen, R.A., Fabricant, D., Franx, M., Caldwell, N., 2000, ApJS 126, 331
de Jong R.S, van der Kruit P.C., 1994, A&AS 106, 451
Kannappan, S. J., Fabricant, D.G., Franx, M. 2002, AJ 123, 2358
Karachentsev, I.D., 1972, Soob. Sb. Astr. Observatory Akad, Nauk, 7
Keel, W.C., 1984, ApJ 282, 75
Keel, W.C., 1993, AJ 196, 1771
Keel, W.C., 1996, ApJSS 106, 27
Kennicutt, R.C., Jr. et al. 1987, AJ 93, 1011
Kennicutt, R.C., Jr., 1983, ApJ 272, 54
Kennicutt, R.C., Jr., Tamblyn, P., Congdon, C.E., 1994, ApJ 435, 22
Kraan-Korteweg, R.C., 1986, A&AS 66, 255
Márquez I. PhD Thesis. 1994. Universidad de Granada.
Márquez I., Moles M., 1994, AJ 108, 90
Márquez I., Moles M., 1996, A&AS 120, 1 **(Paper I)**
Márquez I., Moles M., 1999, A&A 344, 421 **(Paper II)**
Masegosa,J., Moles, M., Campos-Aguilar, A., 1994, ApJ 420, 576
Mathewson, D.S., Ford, V.L., Buchorn, M., 1992, ApJS 81, 413
McCall,M. L., Rybski, P. M., Shields, G. A., 1985, ApJS 57, 1
Moles M., Márquez I., Pérez E., 1995, ApJ 438, 604
Mihos, J.C., Hernquist, L., 1996, ApJ 464, 641
Oey, M.S., Kennicutt, R.C., Jr., 1993, ApJ 411, 137
Persic, M., Salucci, P., Stel, F., 1996, MNRAS 281, 27
Peterson Ch.J., Rubin, V.C., Ford, W.K., Roberts, M.S., 1978, ApJ 226, 770
Rubin, V.C., Hunter, D., Ford, W.K., 1991, ApJS 76, 153
Rubin, V.C., Kenney, J.D.P., Young, J.S., 1997, AJ 113, 1250
Rubin, V.C., Waterman, A.H., Kenney, J.D.P., 1999, AJ 118, 236
Stasinska, G., Sodré, L., 2001, A&A 374, 919
Sofue, Y., 1998, ApSS 269, 593
Sundelius, B., Thomasson, M., Valtonen, M.J., Byrd, G.G., 1987, A&A 174, 67
Tully, R.B., Pierce, M.J., 2000, ApJ 533, 744
van Zee, L., Salzer, J.J., Haynes, M.P., O'Donoghe, A.A., Balonek, T.J., 1998, AJ 116, 2805
Veilleux, S., Osterbrock, D.E., 1987, ApJS 63, 295
Vila-Costas, M.B., Edmunds, M.G., 1993, MNRAS 265, 199
Zaritsky, D., Kennicutt, R.C., Jr., Huchra, J.P., 1994, ApJ 420, 87

Table 1. Observations

Telescope	Date	Instrument	Spectral res. (Å/pix)	Range (Å)	Slit width (arcsec)	Spatial res. (arcsec/pix)	Average seeing (arcsec)
2.2m CAHA	June 1991	Boller& Chivens	1.31	5926 - 7151	1.5	1.35	1.2 - 1.5
2.2m CAHA	March 1993	Boller& Chivens	1.36	5736 - 7138	1.5	1.69	1.1 - 1.4
INT	Febr. 1993	IDS	0.79	6000 - 7000	1.5	0.65	1.1
ASIAGO	1996, 1997	Boller& Chivens	0.96	5000 - 7000	2.5	1.16	1.4 - 2.4

Table 2. Detailed log of the spectra

Galaxy	Date	PA	Time	RMS	Galaxy	Date	PA	Time	RMS
NGC 828	02/16/93	100	3600	1.4	NGC 493	29/10/97	58	3600	1.5
NGC 2460	02/16/93	40	3600	2.0	NGC 658	28/10/97	20	2983	2.1
NGC 2543	02/12/93	45	3600	4.9	NGC 864	05/10/96	20	3600	1.9
	02/17/93	145	3600	3.1	NGC 1036	30/12/97	5	1803	3.0
NGC 2552	02/17/93	45	3600	1.4	NGC 1137	05/10/96	20	1463	2.8
NGC 2608	03/27/93	60	3000	1.0	NGC 1507	28/12/97	11	3600	1.6
NGC 2633	03/26/93	175	3000	0.6	NGC 1530	27/12/97	23	3600	0.9
NGC 2701	03/28/93	23	3600	1.3		27/12/97	113	3600	1.3
NGC 2748	03/29/93	38	3000	1.9	NGC 2344	28/12/97	0	3600	2.5
NGC 2770	03/26/93	148	3000	0.5		28/12/97	90	3600	3.0
NGC 2964	03/30/93	97	3000	0.5	NGC 2424	29/01/96	81	3600	2.5
NGC 2998	03/29/93	53	3000	0.4	NGC 2469	29/01/96	40	3600	3.4
NGC 3041	03/28/93	95	3600	0.4	NGC 2545	05/06/97	170	3600	1.8
NGC 3183	03/29/93	170	3000	0.3	NGC 2628	31/10/97	177	3600	4.0
NGC 3320	02/12/93	20	3600	3.1		31/10/97	87	2000	2.9
NGC 3370	02/14/93	148	3600	2.5	NGC 2906	11/04/97	75	3600	2.5
NGC 3395	03/29/93	50	1800	0.7		11/04/97	120	3600	3.0
NGC 3396	03/28/93	100	3600	0.5	NGC 3044	04/03/97	114	3600	3.1
NGC 3471	02/13/93	14	3600	4.4	NGC 3055	12/04/97	63	3428	2.5
NGC 3501	03/30/93	25	3000	1.0		12/04/97	83	3600	1.9
NGC 3507	03/27/93	110	3000	0.4	NGC 3526	05/03/97	55	3600	0.9
NGC 3689	02/13/93	97	3600	3.0	NGC 4455	05/03/97	16	3600	1.6
NGC 3769a	03/31/93	110	3000	0.3	NGC 5147	14/04/96	0	3600	2.6
NGC 3769	03/31/93	152	3000	1.0	NGC 5375	12/04/97	0	3600	0.6
NGC 3976	03/27/93	53	3000	1.0	NGC 5894	12/04/97	13	3600	3.0
NGC 4047	02/16/93	105	3600	3.5	NGC 5908	05/03/97	154	2339	2.1
NGC 4284	03/29/93	102	3600	0.5	IC 391	28/12/97	0	3600	0.8
NGC 4389	03/28/93	105	3000	0.5	IC 396	29/12/97	85	3600	1.5
NGC 4496a	02/17/93	70	3200	10		29/12/97	175	3600	2.0
NGC 4496b	03/27/93	115	3000	1.0	UGC 1155	28/10/97	165	3600	0.8
NGC 4793	02/13/93	50	3600	1.7	UGC 3580	29/12/97	3	3600	3.0
NGC 4800	03/27/93	25	3000	0.5	UGC 4107	29/10/97	40	3600	2.6
NGC 5012	06/22/91	10	1800	4.3		29/10/97	130	3600	1.9
	06/17/91	170	1800	6.5	UGC 11577	28/10/97	90	3600	3.0
NGC 5172	06/19/91	103	2500	3.3	UGC 12178	29/10/97	20	3600	1.9
	06/19/91	13	1000	3.1	UGC 12857	05/10/96	34	3600	2.4
NGC 5351	06/20/91	150	2000	4.2					
	06/22/91	10	1000	6.0					
NGC 5394	06/18/91	145	1000	19					
	06/23/91	55	1200	20					
NGC 5395	06/19/91	170	2000	3.9					
NGC 5480	06/22/91	177	1500	5.5					
	06/22/91	87	1000	6.5					
NGC 5533	06/21/91	30	1800	4.5					
NGC 5641	06/19/91	158	2000	4.3					
NGC 5656	06/21/91	50	2000	3.3					
	06/22/91	140	1000	4.9					
NGC 5678	06/21/91	5	1800	2.9					
NGC 5740	06/21/91	160	2000	2.2					
NGC 5774	06/20/91	142	2000	4.5					
NGC 5775	06/20/91	146	1800	4.2					
NGC 5899	06/18/91	18	2000	10					
	06/17/91	162	2500	5.1					
NGC 5963	06/19/91	45	2000	4.9					
	06/22/91	135	1200	7.1					
NGC 5970	06/21/91	88	1800	5.9					
	06/23/91	178	953	7.5					
NGC 6070	06/17/91	62	2500	9.3					
	06/23/91	152	1200	1.6					
NGC 6106	06/20/91	140	1800	6.7					
	06/22/91	50	1000	4.5					
NGC 6181	06/20/91	175	2000	5.8					
NGC 6207	06/21/91	22	1402	9.0					
NGC 6239	06/18/91	118	2000	6.0					
NGC 7177	06/18/91	90	2000	4.5					
	06/23/91	0	1200	6.7					
NGC 7217	06/24/91	100	1200	3.7					
	06/22/91	10	1200	3.9					
NGC 7448	06/21/91	170	1800	5.5					
NGC 7479	06/24/91	45	1200	5.2					
	06/24/91	135	1200	6.4					

February 1993: INT telescope; 1996, 1997: Asiago, otherwise: 2.2m CAHA telescope.

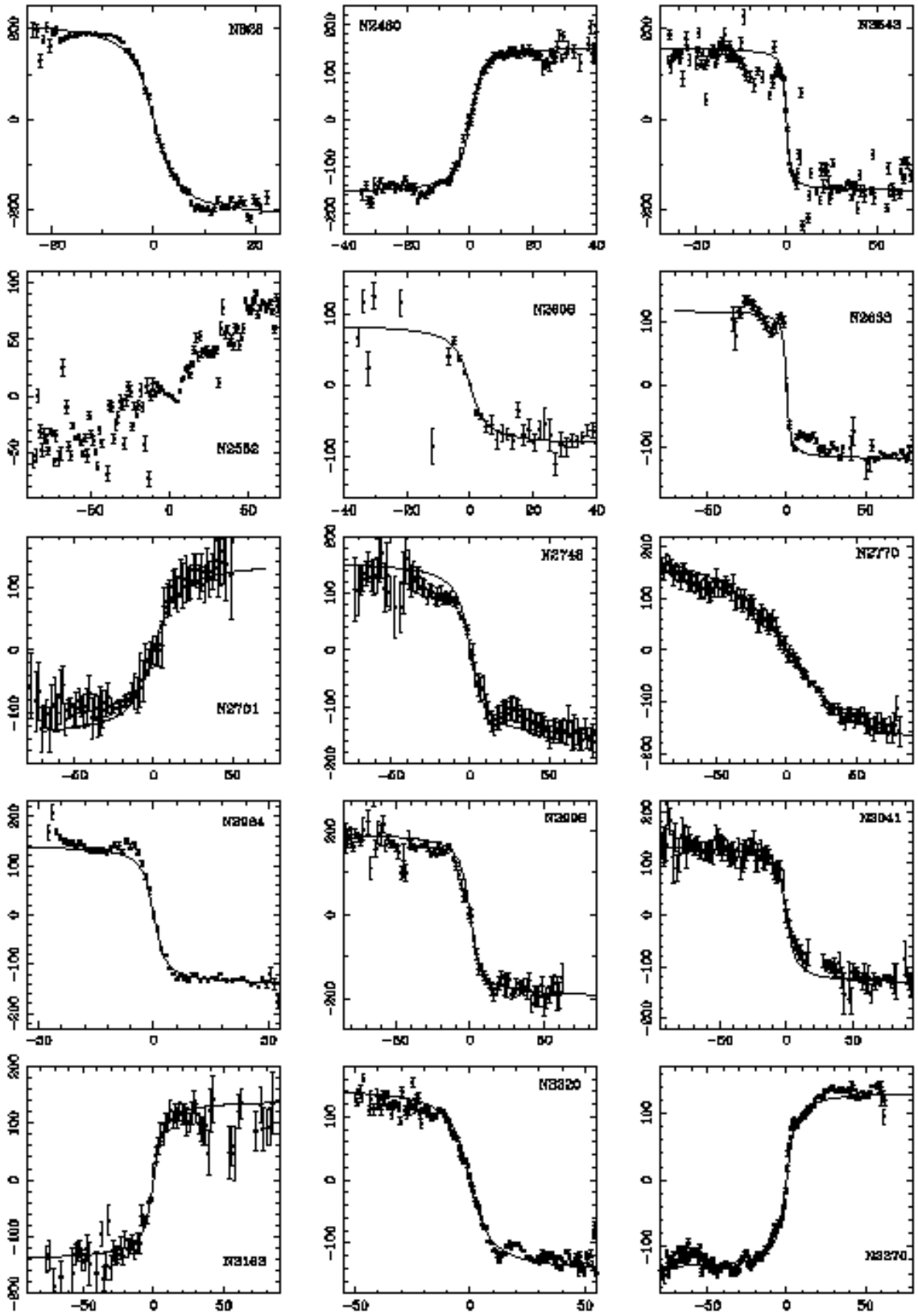

Fig. 4. Rotation curves from INT and CAHA spectra. Velocities are in km/s (y axis) and distances to the center in arcseconds.

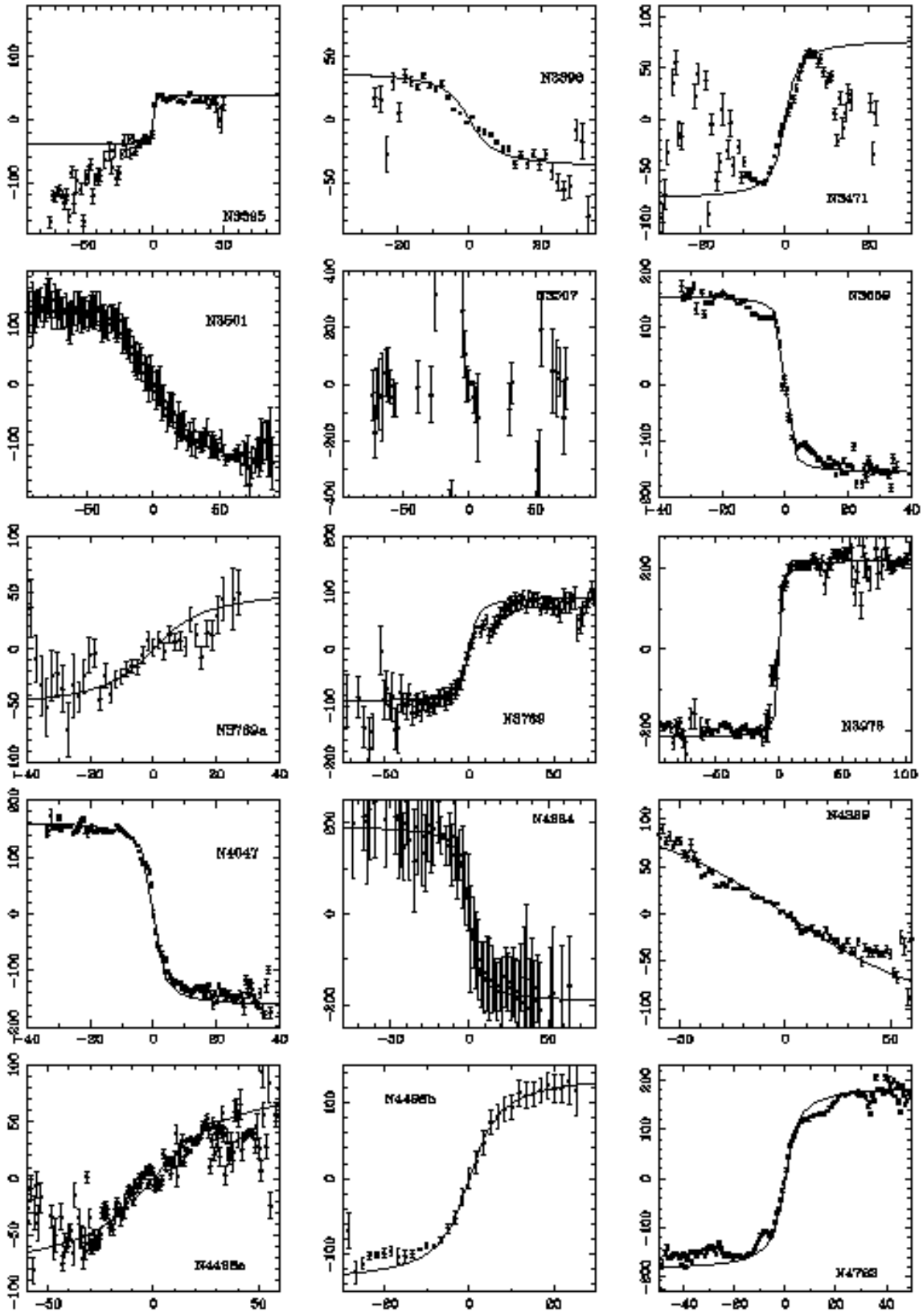

Fig. 4. Rotation curves from INT and CAHA spectra (cont.).

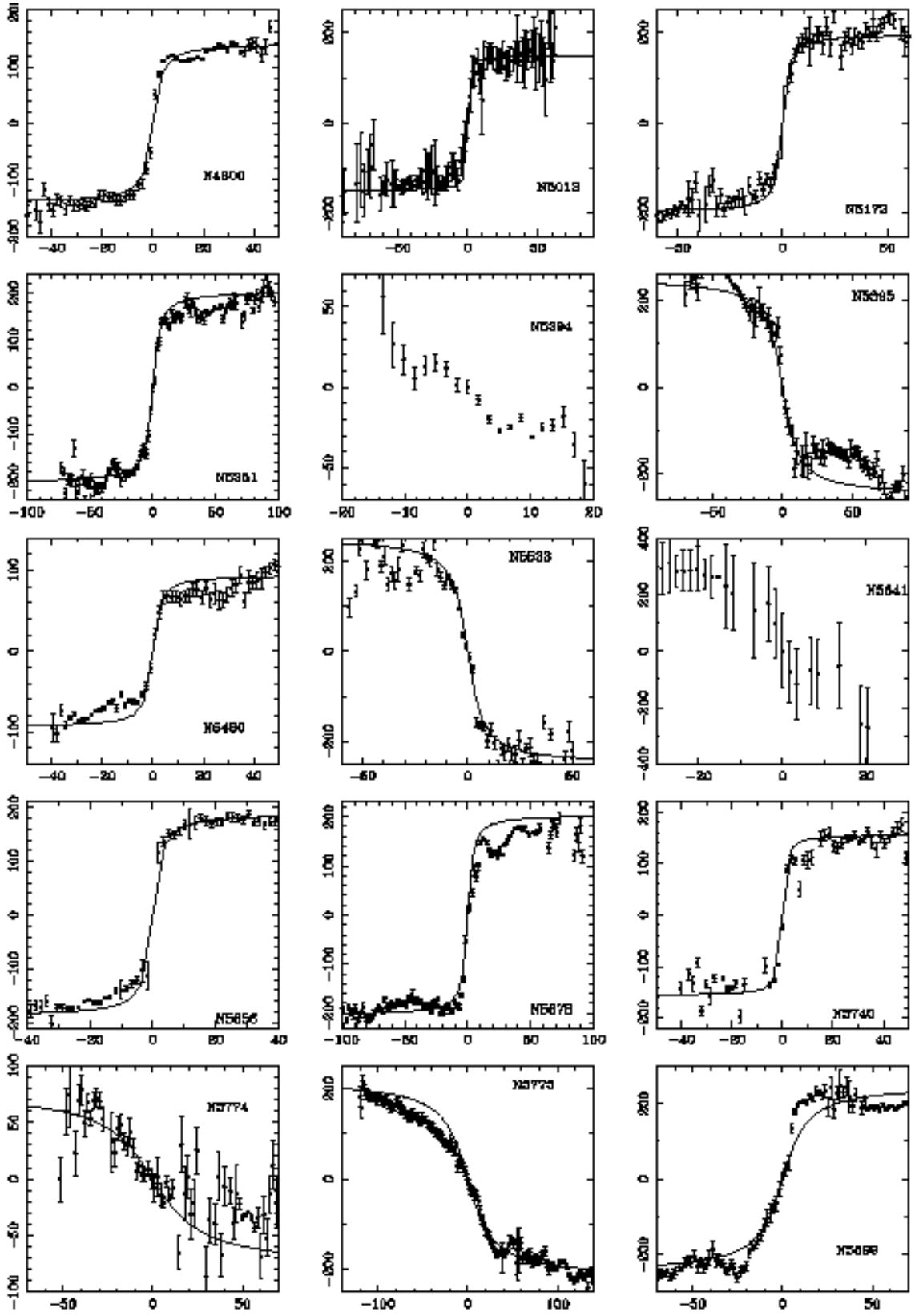

Fig. 4. Rotation curves from INT and CAHA spectra (cont.).

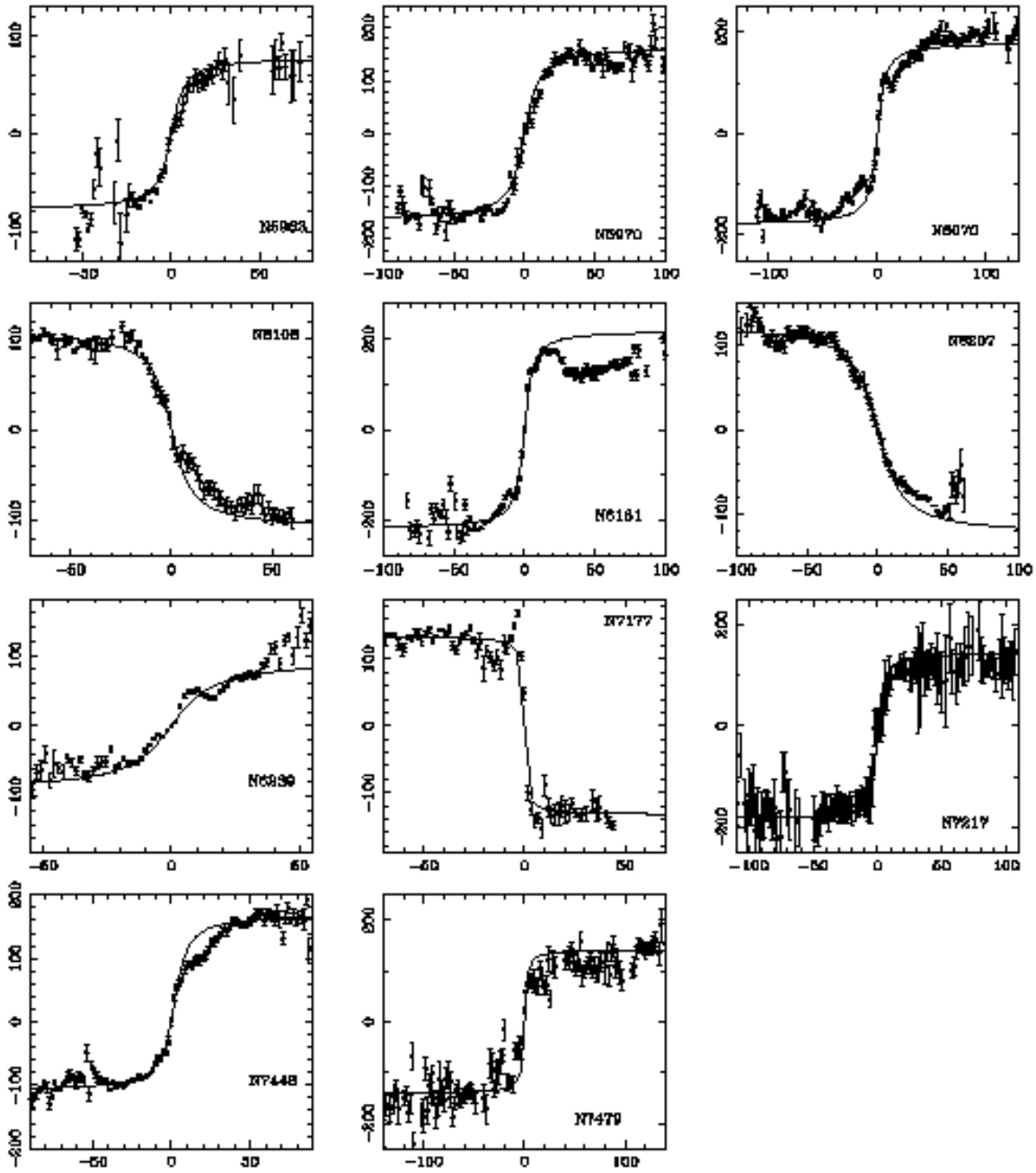

Fig. 4. Rotation curves from INT and CAHA spectra (cont.).

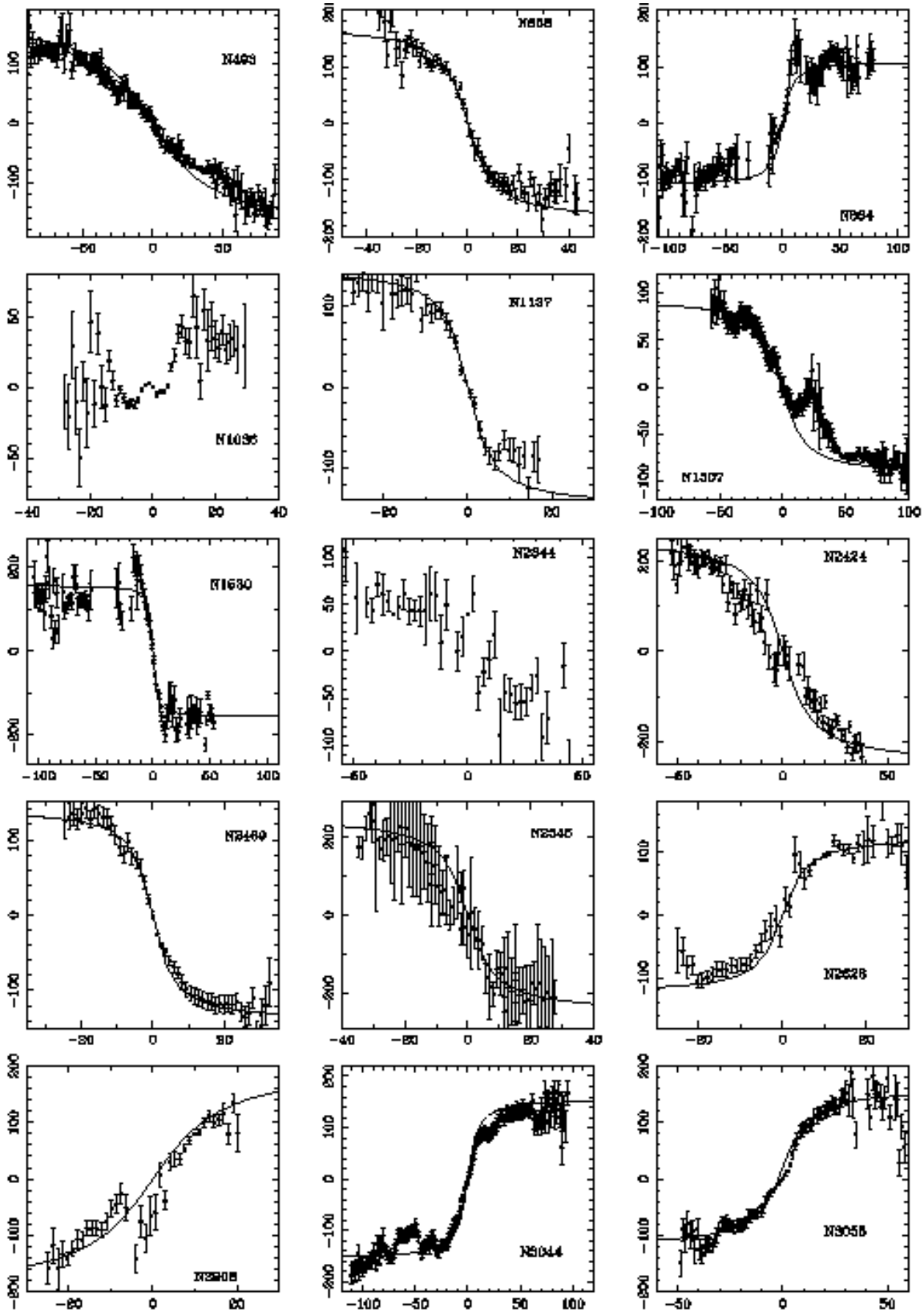

Fig. 5. Rotation curves from Asiago spectra.

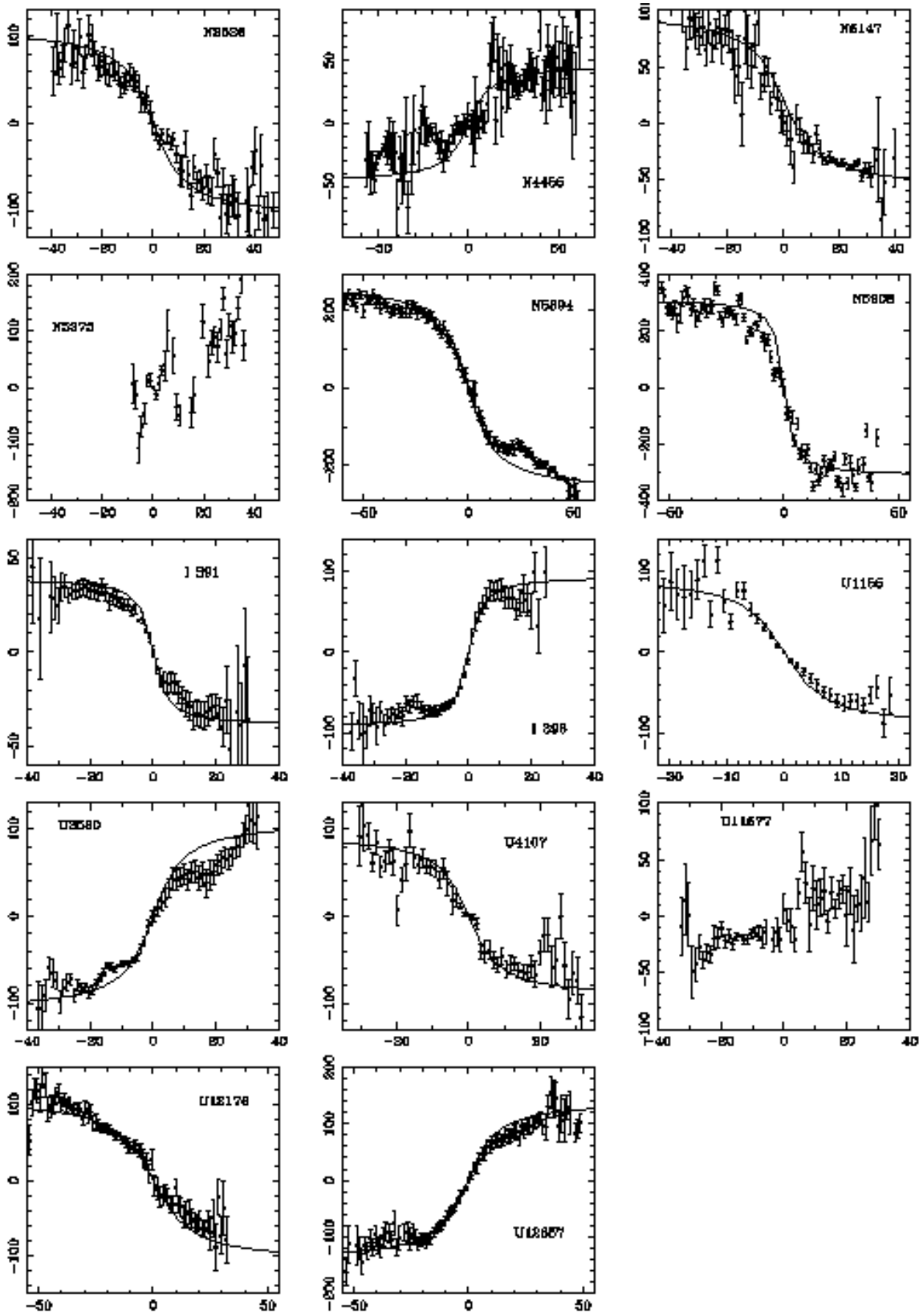

Fig. 5. Rotation curves from Asiago spectra (cont.).

Table 3. Parameters derived from the mayor axes velocity distributions

Galaxy	m_B(RC3) (mag)	t	i	D_{25}	r_G (arcsec)	v_G (km/s)	r_1 (arcsec)	v_1 (km/s)	r_m (arcsec)	v_m (km/s)	INT	Shape	cz (km/s)	D (Mpc)
NGC 828	12.87	1.0	0.17	1.46	0.98	47.0	10.0	195.0	23.0	175.0	2	1	5383	73.4
NGC 2460	12.34	1.0	0.12	1.39	2.9	74.0	14.0	154.0	28.0	146.0	3	2	1462	24.1
NGC 2543*	12.14	3.0	0.24	1.37	0.97	64.0	5.00	125.0	75.0	145.0	2	4	2478	36.2
NGC 2552	12.21	9.0	0.18	1.54	5.4	7.00	16.0	42.00	69.0	64.00	2	5	519	6.7
NGC 2608	12.55	4.0	0.22	1.36	1.7	29.0	30.0	106.0	35.5	71.00	2	5	2167	31.5
NGC 2633	12.31	3.0	0.20	1.39	1.8	83.0	5.00	103.0	34.0	110.0	3	4	2199	34.8
NGC 2701	12.32	5.0	0.13	1.34	1.6	6.00	26.0	110.0	46.0	113.0	2	2	2334	35.5
NGC 2748	11.59	4.0	0.42	1.48	2.0	4.80	8.00	113.0	46.0	138.0	2	2	1499	25.2
NGC 2770	11.76	5.0	0.52	1.58	1.8	8.00	34.0	122.0	90.0	165.0	2	1	1988	29.8
NGC 2964	11.64	3.0	0.26	1.46	3.4	72.0	12.0	135.0	46.0	156.0	3	4	1336	21.5
NGC 2998	12.53	5.0	0.33	1.46	2.5	54.0	16.0	174.0	62.0	172.0	3	2	4805	67.1
NGC 3041	11.94	5.0	0.19	1.57	2.3	49.0	25.0	139.0	94.0	134.0	2	2	1418	21.8
NGC 3183	12.18	4.0	0.23	1.37	1.7	40.0	12.0	118.0	76.0	136.0	3	3	3122	45.9
NGC 3320	12.48	6.0	0.35	1.34	1.0	23.0	13.0	111.0	50.0	129.0	2	1	2333	35.8
NGC 3370	11.87	5.0	0.25	1.50	2.1	57.0	33.0	138.0	57.0	126.0	1	1	1275	22.8
NGC 3395	12.09	6.0	0.23	1.32	0.90	24.0	4.00	39.00	0.00	0.000	3	5	1698	26.4
NGC 3396	12.29	10.	0.42	1.49	2.6	7.00	13.0	36.00	30.0	13.00	3	4	1708	26.7
NGC 3471	12.87	1.0	0.32	1.24	1.4	14.0	5.50	65.00	16.0	18.00	2	3	2130	33.2
NGC 3501	12.27	5.0	0.88	1.59	1.7	15.0	55.0	125.0	90.0	126.0	3	2	1159	19.2
NGC 3507	11.63	3.0	0.07	1.53	–	–	–	–	–	–	3	5	973	13.1
NGC 3689	12.80	5.0	0.17	1.22	1.6	68.0	19.0	155.0	32.0	157.0	2	3	2700	40.0
NGC 3769	11.78	3.0	0.50	1.49	1.7	15.0	32.0	96.00	73.0	97.00	3	4	751	13.1
NGC 3769A	14.70	9.0	0.38	1.03	–	–	–	–	–	–	3	5	830	15.9
NGC 3976	11.67	3.0	0.50	1.58	3.0	180.	13.0	211.0	106.	210.0	3	1	2538	36.4
NGC 4047	12.83	3.0	0.07	1.20	1.3	67.0	12.0	150.0	32.0	147.0	2	1	3445	49.4
NGC 4284	13.75	4.0	0.33	1.40	1.1	52.0	20.0	186.0	53.0	192.0	2	2	4244	58.2
NGC 4389	12.23	4.0	0.29	1.42	0.90	2.60	7.50	16.00	65.0	107.0	3	3	712	12.2
NGC 4496A	12.00	9.0	0.10	1.60	–	–	31.0	55.00	68.0	70.00	2	4	1727	27.2
NGC 4496B	0.000	10.	0.03	1.01	5.1	71.0	12.0	105.0	25.0	115.0	2	1	4539	58.5
NGC 4793	11.86	5.0	0.27	1.44	1.3	44.0	8.00	120.0	56.0	155.0	3	4	2487	37.8
NGC 4800	12.21	3.0	0.13	1.20	3.0	85.0	8.00	124.0	41.0	140.0	2	3	902	13.3
NGC 5012	12.32	5.0	0.24	1.46	4.0	49.0	42.0	220.0	70.0	179.0	2	2	2635	40.7
NGC 5172	11.99	4.0	0.29	1.52	4.7	166.	40.0	240.0	53.0	235.0	2	1	4076	57.0
NGC 5351*	12.48	3.0	0.28	1.47	2.7	94.0	14.0	164.0	53.0	186.0	3	2	3665	52.7
NGC 5394*	13.90	3.0	0.25	1.24	–	–	–	–	–	–	3	5	3460	46.8
NGC 5395	12.11	3.0	0.27	1.46	2.7	104.	12.0	177.0	54.0	225.0	3	4	3496	51.8
NGC 5480*	12.54	5.0	0.18	1.24	2.0	46.0	4.70	66.00	32.0	86.00	3	2	1887	30.4
NGC 5533	12.39	2.0	0.21	1.49	2.0	40.0	13.0	226.0	41.0	226.0	3	4	3856	55.7
NGC 5641	12.73	2.0	0.26	1.39	2.7	144.	1.70	144.0	16.0	282.0	3	5	4320	63.3
NGC 5656*	12.59	2.0	0.13	1.28	1.4	114.	18.0	170.0	31.0	170.0	3	2	3177	47.2
NGC 5678	11.68	3.0	0.31	1.52	4.0	127.	10.0	180.0	84.0	187.0	3	4	1940	36.2
NGC 5740	12.07	3.0	0.29	1.47	3.0	120.	4.00	120.0	32.0	141.0	3	2	1579	24.7
NGC 5774	13.01	7.0	0.09	1.48	–	–	5.00	110.0	89.0	161.0	3	5	1544	24.7
NGC 5775	11.25	5.0	0.62	1.62	4.0	28.0	32.0	142.0	96.0	209.0	3	4	1707	24.8
NGC 5899*	11.78	5.0	0.43	1.50	2.6	53.0	19.0	239.0	56.0	227.0	3	4	2621	39.1
NGC 5963*	12.76	1.0	0.11	1.52	2.7	25.0	9.00	60.00	50.0	65.00	2	4	663	13.8
NGC 5970	11.85	5.0	0.17	1.46	2.6	41.0	17.0	149.0	70.0	148.0	3	3	1968	31.3
NGC 6070	11.58	6.0	0.30	1.55	0.85	35.5	7.00	110.0	100.	190.0	3	3	1995	29.9
NGC 6106	12.29	5.0	0.30	1.40	2.0	35.0	20.0	110.0	58.0	110.0	1	4	1459	22.9
NGC 6181	11.85	5.0	0.35	1.40	2.7	118.	19.0	184.0	53.0	174.0	2	4	2401	35.6
NGC 6207	11.59	5.0	0.36	1.47	5.3	38.0	24.0	95.00	54.0	106.0	2	2	835	16.0
NGC 6239	12.44	3.0	0.45	1.41	2.7	28.0	10.0	47.00	40.0	84.00	2	1	935	17.6
NGC 7177*	11.50	3.0	0.19	1.49	1.8	102.	3.00	148.0	68.0	148.0	1	4	1118	18.5
NGC 7217*	10.52	2.0	0.08	1.59	–	–	5.00	138.0	86.0	183.0	3	1	950	16.5
NGC 7448	11.48	4.0	0.34	1.43	2.7	52.0	31.0	133.0	68.0	135.0	1	4	2120	32.0
NGC 7479*	11.21	5.0	0.12	1.61	1.4	52.0	39.0	138.0	107.	154.0	1	4	2334	33.7

* Galaxies showing evidences of non-circular motions.

Table 4. Parameters derived from the mayor axes velocity distributions

Galaxy	m_B(RC3) (mag)	t	i	D_{25}	r_G (arcsec)	v_G (km/s)	r_1 (arcsec)	v_1 (km/s)	r_m (arcsec)	v_m (km/s)	INT	Shape	cz (km/s)	D (Mpc)
NGC 493	12.01	6.0	0.62	1.53	2.0	11.7	32.0	94.00	74.0	138.0	2	1	2354	31.7
NGC 658	12.58	3.0	0.28	1.48	1.5	30.9	20.0	138.0	34.0	112.0	1	4	2990	40.8
NGC 864	11.26	5.0	0.12	1.67	1.0	5.90	12.0	136.0	91.0	107.0	2	5	1543	21.7
NGC 1036	13.75	10.	0.14	1.16	–	–	–	–	–	–	1	5	800	12.7
NGC 1137	12.61	3.0	0.21	1.33	0.50	7.90	11.0	126.0	26.0	150.0	1	4	3028	40.2
NGC 1507	11.82	9.0	0.62	1.56	2.5	14.0	44.5	84.00	84.0	87.00	1	5	888	12.0
NGC 1530*	11.42	3.0	0.28	1.66	2.5	69.0	9.50	192.0	114.	157.0	1	4	2496	37.5
NGC 2344	12.48	5.0	0.01	1.23	–	–	–	–	–	–	2	4	990	17.1
NGC 2424	12.19	3.0	0.80	1.58	0.50	1.40	28.5	207.0	45.5	217.0	3	5	3365	45.6
NGC 2469	13.12	4.0	0.17	1.05	2.0	42.0	14.0	128.6	27.0	119.6	1	1	3505	48.0
NGC 2545	12.66	2.0	0.24	1.30	1.0	151.	2.00	196.0	30.0	183.0	2	1	3414	46.8
NGC 2628	13.85	5.0	0.02	1.06	0.50	29.0	10.5	99.00	24.5	105.5	1	3	3609	47.5
NGC 2906*	12.97	6.0	0.23	1.16	1.5	56.0	4.50	98.00	21.5	95.40	1	5	2168	26.1
NGC 3044	11.13	5.0	0.85	1.69	3.0	22.0	38.0	138.0	95.0	179.0	2	3	1313	20.4
NGC 3055	12.18	5.0	0.21	1.32	2.0	11.7	28.0	148.0	46.0	143.0	2	4	1827	27.9
NGC 3526	12.79	5.0	0.65	1.28	2.0	27.0	13.0	72.00	38.0	111.0	1	2	1425	22.6
NGC 4455	12.12	7.0	0.53	1.44	1.0	11.0	12.0	48.00	53.0	60.00	1	5	621	6.6
NGC 5147	12.29	8.0	0.09	1.28	1.0	6.30	8.00	54.00	31.0	77.00	2	3	1083	18.5
NGC 5375	12.29	2.0	0.07	1.51	–	–	–	–	–	–	2	5	2391	36.7
NGC 5894	12.33	8.0	0.85	1.48	1.0	28.0	16.0	174.0	51.0	223.0	2	3	2483	38.6
NGC 5908	12.29	3.0	0.43	1.51	1.0	62.0	16.0	305.0	45.0	325.0	3	4	3331	49.2
IC 391	12.56	5.0	0.02	1.06	1.0	7.90	11.0	31.50	28.0	28.00	1	1	1587	26.0
IC 396	12.08	10.	0.16	1.32	1.0	24.3	8.00	74.70	30.0	76.00	1	2	882	14.9
UGC 1155	14.17	6.0	0.24	0.850	5.0	46.9	10.0	87.00	18.0	70.00	1	3	3188	44.6
UGC 3580	12.20	1.0	0.28	1.53	1.5	10.7	6.50	48.80	29.5	90.60	2	4	1198	21.0
UGC 4107	13.52	5.0	0.01	1.15	1.0	1.54	9.00	58.90	26.0	82.50	1	4	3486	47.1
UGC 11577	13.44	6.0	0.12	1.21	–	–	–	–	–	–	1	5	3767	52.5
UGC 12178	13.13	8.0	0.26	1.47	0.50	17.3	23.5	89.60	48.5	109.4	2	2	1936	28.8
UGC 12857	13.40	4.0	0.68	1.26	2.0	23.4	17.0	95.00	45.0	112.0	2	3	2474	35.5

* Galaxies showing evidences of non-circular motions.

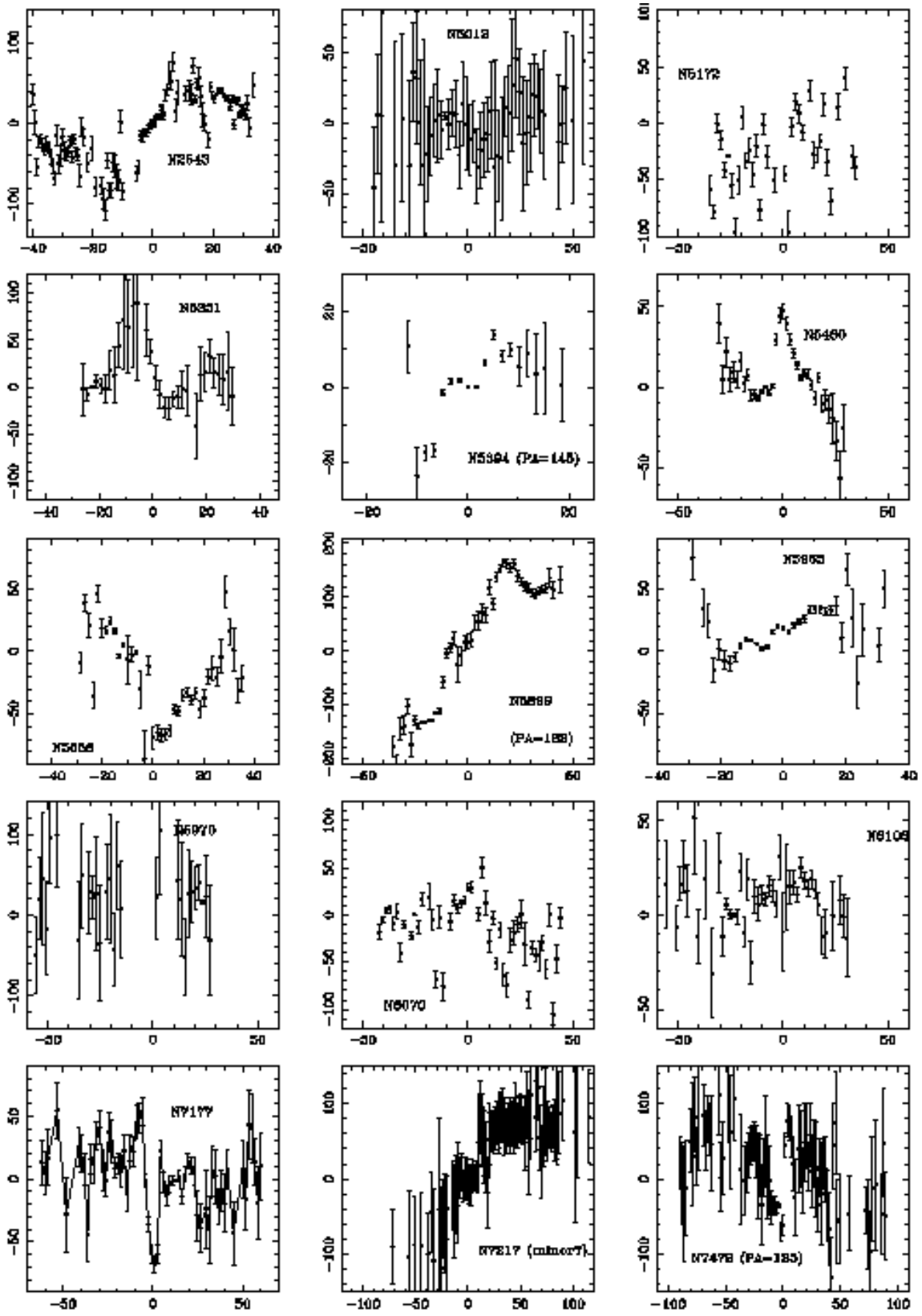

Fig. 6. Velocity distributions for additional PAs (minor axes, otherwise the PA is given) from INT and CAHA spectra.

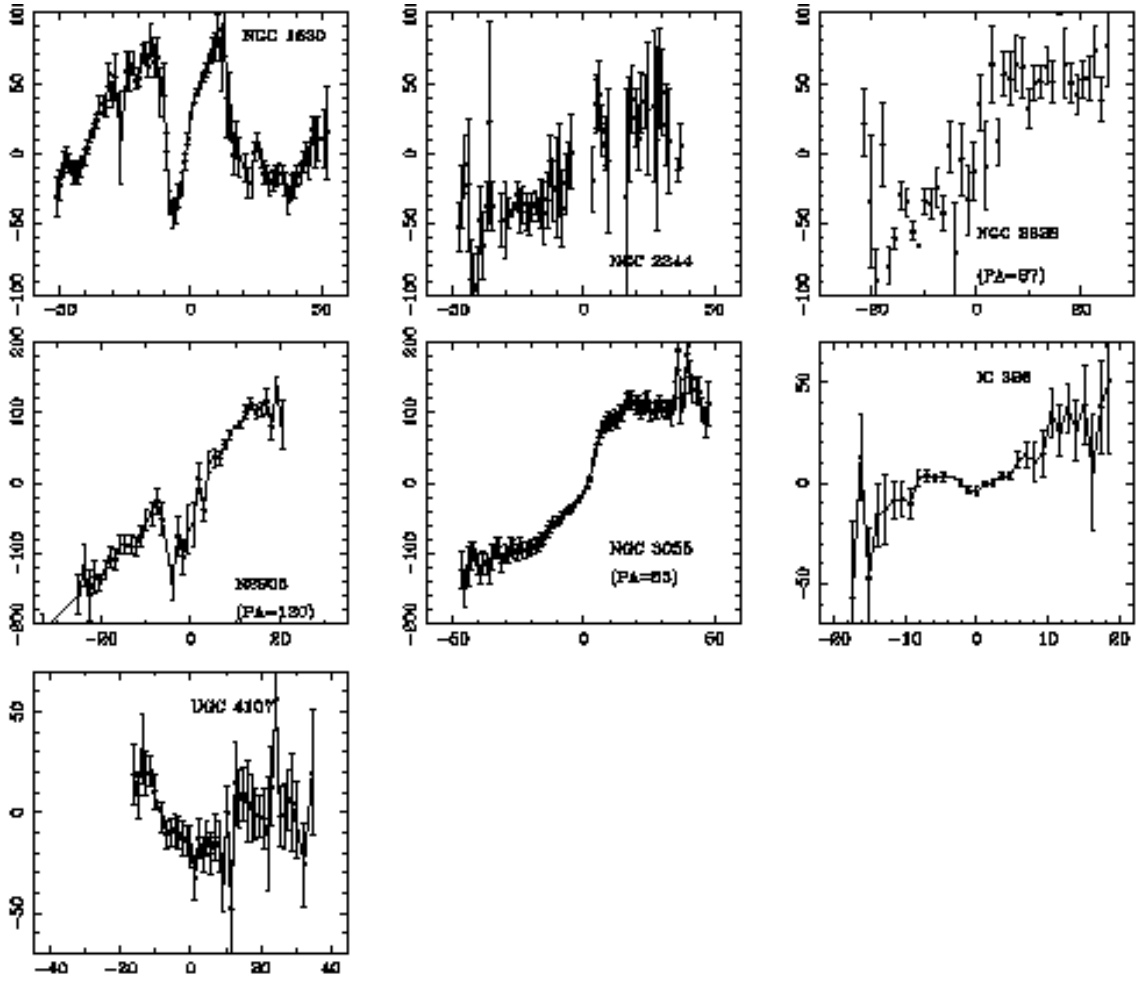

Fig. 7. Velocity distributions for additional PAs (minor axes, otherwise the PA is given) from Asiago spectra.

Table 5. Parameters of the HII regions

Galaxy	R (")	EW(Hα) (Å)	[OI]/Hα	err([OI]/Hα)	[NII]/Hα	err([NII]/Hα)	[SII]/Hα	err([SII]/Hα)	S1/S2
NGC 493	0.0	36.590	–	–	0.290	0.054	–	–	–
NGC 493	-24.4	36.020	–	–	0.138	0.037	–	–	–
NGC 493	-8.1	60.180	–	–	0.181	0.038	–	–	–
NGC 493	13.9	42.810	–	–	0.206	0.075	–	–	–
NGC 493	37.1	63.570	–	–	0.253	0.039	–	–	–
NGC 493	56.8	44.140	–	–	0.269	0.059	–	–	–
NGC 493	66.1	365.600	–	–	0.219	0.026	–	–	–
NGC 658	0.0	15.300	–	–	0.396	0.042	–	–	–
NGC 658	-11.6	20.460	–	–	0.312	0.056	–	–	–
NGC 658	16.2	35.160	–	–	0.289	0.100	–	–	–
NGC 828	0.0	13.830	–	–	0.510	0.029	0.225	0.052	0.863
NGC 828	-7.8	43.570	–	–	0.433	0.031	0.288	0.055	1.159
NGC 864	0.0	44.200	–	–	0.409	0.017	0.336	0.031	0.919
NGC 864	-95.1	264.400	–	–	0.158	2.057	0.375	4.113	1.566
NGC 864	-61.5	657.800	–	–	0.193	1.863	–	–	–
NGC 864	-49.9	296.300	–	–	0.224	1.581	–	–	–
NGC 864	-41.8	163.000	–	–	0.327	5.373	–	–	–
NGC 864	40.6	440.800	–	–	0.361	2.021	0.323	4.043	1.485
NGC 1036	0.0	67.740	0.015	0.014	0.168	0.015	0.287	0.030	1.320
NGC 1036	-11.6	138.800	0.014	0.009	0.127	0.010	0.201	0.020	1.306
NGC 1137	0.0	11.450	–	–	0.376	0.061	–	–	–
NGC 1137	4.6	19.530	–	–	0.398	0.087	–	–	–
NGC 1507	0.0	20.320	–	–	0.172	0.036	0.478	0.072	1.365
NGC 1507	-27.8	54.320	–	–	0.110	0.021	0.247	0.043	1.453
NGC 1507	-19.7	47.910	–	–	0.153	0.030	0.391	0.061	1.310
NGC 1507	-8.1	38.710	–	–	0.119	0.029	0.308	0.058	1.501
NGC 1507	9.3	84.570	–	–	0.141	0.016	0.237	0.032	1.370
NGC 1507	47.6	121.200	–	–	0.099	0.020	0.304	0.041	1.461
NGC 1507	62.6	293.200	–	–	0.077	0.048	0.297	0.097	1.138
NGC 1507	85.8	-28.760	–	–	–	–	0.251	0.165	1.589
NGC 1530	0.0	36.740	0.010	0.009	0.345	0.011	0.181	0.019	1.260
NGC 1530	-74.2	68.040	–	–	0.225	0.053	0.285	0.103	1.526
NGC 1530	-62.6	385.400	–	–	0.333	0.081	0.323	0.159	1.415
NGC 2344	0.0	0.000	–	–	–	–	–	–	–
NGC 2344	-31.3	69.610	–	–	0.269	0.108	–	–	–
NGC 2344	8.1	4.079	–	–	0.381	0.161	–	–	–
NGC 2424	0.0	0.000	–	–	–	–	–	–	–
NGC 2424	-34.8	232.300	–	–	0.317	0.088	–	–	–
NGC 2424	25.5	44.750	–	–	0.374	0.071	–	–	–
NGC 2460	0.0	0.520	0.317	0.318	3.301	0.330	1.604	0.640	0.864
NGC 2460	-24.1	16.560	0.191	0.090	0.522	0.095	0.463	0.181	1.060
NGC 2460	-12.3	5.880	–	–	0.691	0.092	0.545	0.175	1.233
NGC 2460	-8.5	5.630	–	–	0.789	0.084	0.459	0.155	0.958
NGC 2460	3.3	1.310	–	–	1.748	0.107	0.953	0.204	0.851
NGC 2460	9.1	10.310	–	–	0.518	0.038	0.362	0.070	1.070
NGC 2460	20.2	8.630	–	–	0.569	0.088	0.412	0.167	2.004
NGC 2469	0.0	54.730	0.034	0.090	0.388	0.015	–	–	–
NGC 2469	-12.8	71.730	0.029	0.090	0.262	0.026	–	–	–
NGC 2469	10.4	146.900	0.015	0.090	0.274	0.011	–	–	–
NGC 2543	0.0	31.560	0.009	0.010	0.450	0.011	0.273	0.020	1.267
NGC 2543	-61.8	85.830	–	–	0.267	0.126	0.395	0.251	1.646
NGC 2543	-40.0	27.490	–	–	0.301	0.153	–	–	–
NGC 2543	31.9	15.520	0.036	0.070	0.492	0.076	0.433	0.145	1.389
NGC 2545	0.0	0.000	–	–	–	–	–	–	–
NGC 2545	-16.2	24.810	–	–	0.342	0.073	0.267	0.142	1.551
NGC 2545	16.2	16.950	–	–	0.483	0.125	–	–	–
NGC 2552	0.0	236.900	0.013	0.010	0.092	0.011	0.234	0.022	1.397
NGC 2552	-46.2	43.210	–	–	0.155	0.152	0.278	0.304	0.805
NGC 2552	-20.8	39.180	–	–	0.076	0.203	–	–	–
NGC 2552	-3.9	80.840	–	–	0.125	3.789	0.264	7.578	1.495
NGC 2552	59.8	56.460	–	–	0.034	0.077	0.365	0.160	1.243
NGC 2608	0.0	36.150	0.013	0.019	0.495	0.025	0.334	0.043	1.083
NGC 2608	-6.8	15.250	0.017	0.053	0.535	0.067	0.540	0.121	1.075
NGC 2608	40.6	18.460	–	–	0.498	0.103	0.259	0.186	1.223
NGC 2628	0.0	0.810	–	–	3.398	0.461	–	–	–
NGC 2628	-18.6	49.330	–	–	0.436	0.060	–	–	–
NGC 2628	-9.3	17.320	–	–	0.434	0.069	–	–	–
NGC 2628	10.4	14.130	–	–	0.518	0.065	–	–	–
NGC 2633	0.0	44.370	0.012	0.006	0.530	0.009	0.256	0.014	0.961
NGC 2633	-23.7	24.610	0.028	0.041	0.454	0.050	0.360	0.090	1.366
NGC 2633	-11.8	22.890	0.033	0.035	0.493	0.045	0.373	0.078	1.208
NGC 2633	15.2	16.070	0.029	0.043	0.511	0.053	0.415	0.096	0.647
NGC 2633	65.9	232.500	0.016	0.020	0.183	0.024	0.235	0.045	1.223

Table 5. Parameters of the HII regions (Cont.)

Galaxy	R (")	EW(Hα) (Å)	[OI]/Hα	err([OI]/Hα)	[NII]/Hα	err([NII]/Hα)	[SII]/Hα	err([SII]/Hα)	S1/S2
NGC 2701	0.0	17.030	–	–	0.398	0.038	0.344	0.069	1.379
NGC 2701	-49.0	34.820	–	–	0.137	0.087	0.583	0.180	1.484
NGC 2701	-20.3	32.040	–	–	0.303	0.043	0.435	0.083	1.901
NGC 2701	25.4	25.580	–	–	0.216	0.076	0.274	0.147	1.365
NGC 2748	0.0	17.570	–	–	0.434	0.037	0.363	0.070	1.226
NGC 2748	-25.4	27.100	–	–	0.389	0.058	0.422	0.110	1.160
NGC 2748	-6.8	27.740	–	–	0.365	0.027	0.333	0.048	1.399
NGC 2748	15.2	26.080	0.042	0.034	0.366	0.039	0.339	0.073	1.303
NGC 2748	37.2	34.110	0.018	0.035	0.328	0.040	0.367	0.076	1.176
NGC 2748	52.4	73.520	0.026	0.020	0.295	0.025	0.294	0.045	1.326
NGC 2748	72.7	66.760	0.029	0.038	0.153	0.041	0.154	0.078	1.409
NGC 2770	0.0	13.200	–	–	0.424	0.072	0.670	0.140	1.206
NGC 2770	-86.2	647.700	–	–	0.155	0.086	0.504	0.176	1.088
NGC 2770	-64.2	25.870	–	–	0.277	0.205	–	–	–
NGC 2770	-37.2	22.630	–	–	0.304	0.053	0.522	0.103	1.376
NGC 2770	-21.0	12.950	–	–	0.386	0.084	0.499	0.160	1.435
NGC 2770	-1.7	24.830	–	–	0.365	0.107	0.502	0.207	1.360
NGC 2770	15.2	11.340	–	–	0.450	0.107	0.641	0.204	0.917
NGC 2770	25.3	18.120	–	–	0.423	0.093	0.523	0.175	1.404
NGC 2770	32.1	27.200	–	–	0.372	0.060	0.483	0.113	1.193
NGC 2770	52.4	26.600	–	–	0.276	0.072	0.506	0.142	1.444
NGC 2770	74.4	44.580	–	–	0.169	0.091	0.336	0.183	1.576
NGC 2798	0.0	96.710	0.009	0.004	0.529	0.006	0.228	0.010	1.016
NGC 2798	-10.1	57.940	0.035	0.017	0.477	0.022	0.408	0.038	1.201
NGC 2798	6.8	48.390	0.030	0.016	0.460	0.021	0.376	0.036	1.323
NGC 2799	0.0	75.460	0.009	0.016	0.271	0.020	0.318	0.038	1.335
NGC 2799	-13.5	20.090	–	–	0.314	0.062	0.409	0.120	0.929
NGC 2799	11.8	24.870	–	–	0.274	0.066	0.314	0.126	1.046
NGC 2906	0.0	1.750	–	–	0.250	0.157	–	–	–
NGC 2906	-13.9	10.980	–	–	–	–	–	–	–
NGC 2906	9.3	12.990	–	–	–	–	–	–	–
NGC 2964	0.0	45.350	0.018	0.008	0.486	0.011	0.045	0.017	1.118
NGC 2964	-25.4	33.850	–	–	0.386	0.044	0.308	0.079	1.750
NGC 2964	22.0	18.040	0.051	0.065	0.496	0.077	0.405	0.140	1.200
NGC 2964	37.2	140.900	0.009	0.012	0.342	0.016	0.286	0.028	1.361
NGC 2998	0.0	4.290	–	–	0.579	0.081	0.294	0.145	0.961
NGC 2998	-32.1	92.400	0.030	0.029	0.316	0.036	0.276	0.064	1.465
NGC 2998	-11.8	19.050	–	–	0.365	0.049	0.289	0.090	1.332
NGC 2998	10.1	17.580	0.053	0.046	0.344	0.052	0.220	0.095	1.585
NGC 3041	0.0	3.250	–	–	0.703	0.110	0.261	0.200	1.047
NGC 3041	-64.2	52.830	–	–	0.343	0.094	0.252	0.176	1.167
NGC 3041	6.8	8.500	–	–	0.456	0.078	0.205	0.136	1.334
NGC 3041	33.8	16.890	0.107	0.084	0.435	0.093	0.301	0.170	1.735
NGC 3041	72.7	93.160	0.029	0.040	0.279	0.048	0.292	0.088	1.227
NGC 3044	0.0	89.120	0.026	0.013	0.319	0.015	0.391	0.029	1.531
NGC 3044	-95.1	349.800	–	–	0.087	1.825	0.201	3.649	1.012
NGC 3044	-61.5	242.400	–	–	0.107	0.026	0.178	0.052	1.206
NGC 3044	-51.0	339.300	–	–	0.090	0.038	0.151	0.076	2.285
NGC 3044	-44.1	151.400	–	–	0.141	0.036	0.280	0.072	1.508
NGC 3044	-19.7	222.300	–	–	0.223	0.021	0.328	0.040	1.436
NGC 3044	1.2	107.400	0.033	0.014	0.300	0.016	0.399	0.031	1.505
NGC 3044	25.5	214.000	0.027	0.024	0.252	0.025	0.361	0.050	1.457
NGC 3044	59.2	79.780	–	–	0.254	0.051	0.354	0.100	1.414
NGC 3055	0.0	95.100	0.021	0.007	0.452	0.009	0.289	0.016	1.207
NGC 3055	-17.4	24.120	–	–	0.357	0.109	0.468	0.211	1.459
NGC 3055	30.2	293.900	–	–	0.204	1.117	0.270	2.234	1.313
NGC 3183	0.0	9.800	–	–	1.092	0.061	0.547	0.099	1.233
NGC 3183	-15.2	11.580	–	–	0.509	0.100	0.384	0.181	1.565
NGC 3183	11.8	6.950	–	–	0.619	0.094	0.551	0.173	1.947
NGC 3294	0.0	32.150	0.019	0.032	0.379	0.039	0.338	0.071	1.439
NGC 3294	-69.3	29.330	0.028	0.048	0.452	0.059	0.434	0.107	1.709
NGC 3294	-42.3	33.270	0.028	0.031	0.415	0.038	0.382	0.069	1.563
NGC 3294	-22.0	27.730	0.040	0.042	0.387	0.051	0.362	0.093	1.365
NGC 3294	-11.8	35.170	–	–	0.388	0.050	0.297	0.088	1.466
NGC 3294	18.6	78.980	0.011	0.023	0.356	0.030	0.316	0.053	1.507
NGC 3320	-62.6	17.110	–	–	0.404	1.367	–	–	–
NGC 3320	-54.5	15.420	–	–	0.345	0.275	–	–	–
NGC 3320	-28.0	18.960	–	–	0.268	0.081	0.402	0.160	2.033
NGC 3320	-13.9	21.630	–	–	0.323	0.028	0.287	0.052	1.418
NGC 3320	42.9	31.900	–	–	0.244	0.227	0.489	0.454	1.259
NGC 3320	0.0	11.690	–	–	0.426	0.037	0.305	0.069	1.008
NGC 3320	9.3	18.840	–	–	0.375	0.049	0.312	0.094	1.169
NGC 3320	17.4	26.020	–	–	0.344	0.058	0.295	0.111	1.190
NGC 3320	26.7	9.440	–	–	0.484	0.158	0.836	0.315	1.045
NGC 3320	42.9	24.560	–	–	0.232	0.117	0.435	0.234	1.130
NGC 3320	74.2	21.560	–	–	0.313	0.008	0.363	0.016	1.210
NGC 3320	80.0	27.250	–	–	0.295	0.196	0.252	0.387	1.580

Table 5. Parameters of the HII regions (Cont.)

Galaxy	R (")	EW(Hα) (Å)	[OI]/Hα	err([OI]/Hα)	[NII]/Hα	err([NII]/Hα)	[SII]/Hα	err([SII]/Hα)	S1/S2
NGC 3370	0.0	6.060	–	–	0.461	0.026	0.276	0.050	1.038
NGC 3370	-69.6	256.900	–	–	0.194	1.657	0.294	3.315	1.483
NGC 3370	-57.9	100.600	0.023	0.071	0.194	0.074	0.601	0.151	1.329
NGC 3370	-48.8	42.730	–	–	0.233	0.080	0.491	0.161	1.266
NGC 3370	-40.3	75.550	–	–	0.207	0.023	0.403	0.046	1.551
NGC 3370	18.9	20.300	0.048	0.030	0.378	0.033	0.435	0.064	1.381
NGC 3370	-30.6	55.460	0.032	0.034	0.287	0.037	0.470	0.072	1.371
NGC 3370	-12.3	36.860	0.015	0.014	0.298	0.017	0.291	0.031	1.458
NGC 3370	2.0	6.220	0.029	0.016	0.476	0.019	0.288	0.034	1.084
NGC 3370	10.4	12.480	0.024	0.047	0.407	0.049	0.319	0.095	0.988
NGC 3370	27.3	37.380	0.052	0.053	0.297	0.055	0.465	0.109	1.526
NGC 3370	31.2	65.960	0.049	0.022	0.334	0.026	0.414	0.048	1.116
NGC 3370	36.4	56.680	0.070	0.034	0.260	0.036	0.435	0.072	1.217
NGC 3370	52.7	284.300	0.022	0.016	0.153	0.018	0.258	0.035	1.430
NGC 3395	0.0	143.800	0.012	0.006	0.206	0.007	0.202	0.013	1.298
NGC 3395	-94.6	61.140	–	–	0.254	0.073	0.437	0.143	1.801
NGC 3395	-32.1	292.700	0.018	0.027	0.127	0.028	0.246	0.057	0.979
NGC 3395	-22.0	72.440	0.057	0.046	0.208	0.050	0.442	0.100	1.110
NGC 3396	0.0	155.400	0.012	0.005	0.201	0.006	0.171	0.012	1.249
NGC 3396	-10.1	55.610	0.026	0.019	0.247	0.022	0.369	0.043	1.357
NGC 3396	8.5	123.100	0.023	0.013	0.194	0.015	0.253	0.029	1.368
NGC 3471	0.0	93.080	0.012	0.004	0.410	0.006	0.267	0.010	1.175
NGC 3501	0.0	3.360	–	–	0.589	0.132	0.666	0.252	0.904
NGC 3501	-84.5	27.300	–	–	0.280	0.111	0.409	0.215	2.554
NGC 3501	-67.6	13.100	–	–	0.268	0.103	0.606	0.208	1.430
NGC 3501	-45.6	11.780	0.073	0.078	0.498	0.089	0.604	0.168	1.951
NGC 3501	-30.4	9.830	0.075	0.075	0.435	0.084	0.414	0.157	1.381
NGC 3501	-10.1	6.790	–	–	0.443	0.090	0.442	0.170	1.309
NGC 3501	8.4	3.400	–	–	0.665	0.119	0.654	0.226	0.954
NGC 3501	38.9	10.960	–	–	0.370	0.098	0.594	0.191	1.308
NGC 3501	59.1	42.080	–	–	0.294	0.051	0.363	0.096	1.354
NGC 3507	0.0	6.900	–	–	0.890	0.120	0.849	0.220	0.711
NGC 3526	0.0	35.420	–	–	0.248	0.061	0.609	0.124	1.157
NGC 3526	-16.2	41.290	–	–	0.112	0.060	0.325	0.121	1.499
NGC 3549	0.0	0.730	–	–	2.197	0.432	–	–	–
NGC 3549	-62.6	46.920	–	–	0.387	0.092	–	–	–
NGC 3549	-49.9	31.550	–	–	0.405	0.119	–	–	–
NGC 3549	-25.5	17.590	–	–	0.504	0.066	0.296	0.123	0.884
NGC 3549	-17.4	14.560	–	–	0.373	0.058	0.220	0.108	1.621
NGC 3549	16.2	10.530	–	–	0.405	0.067	0.264	0.127	1.205
NGC 3549	37.1	30.560	–	–	0.386	0.058	0.275	0.111	2.156
NGC 3549	45.2	17.300	–	–	0.408	0.128	0.332	0.249	1.845
NGC 3689	0.0	0.510	0.698	0.332	4.393	0.350	1.649	0.666	0.884
NGC 3689	-18.2	34.900	0.017	0.024	0.375	0.028	0.395	0.052	1.420
NGC 3689	-7.8	20.030	0.025	0.018	0.352	0.021	0.286	0.039	1.094
NGC 3689	8.5	25.780	0.036	0.021	0.358	0.024	0.301	0.044	1.367
NGC 3689	30.6	25.120	0.091	0.078	0.443	0.083	0.472	0.160	1.409
NGC 3769A	0.0	30.300	0.020	0.032	0.362	0.039	0.388	0.072	1.478
NGC 3769A	-8.4	44.570	–	–	0.305	0.036	0.351	0.066	1.462
NGC 3769A	15.2	20.330	–	–	0.362	0.057	0.586	0.111	1.222
NGC 3769A	79.4	64.740	0.020	0.045	0.050	0.046	0.312	0.101	1.451
NGC 3769A	87.9	155.400	0.021	0.114	0.043	0.114	0.232	0.229	1.167
NGC 3769	0.0	9.840	0.052	0.051	0.366	0.056	0.404	0.107	1.898
NGC 3769	-37.2	17.710	–	–	0.338	0.128	0.843	0.261	1.014
NGC 3769	-23.7	24.700	0.011	0.050	0.343	0.060	0.541	0.117	1.442
NGC 3769	-10.1	12.660	–	–	0.338	0.068	0.451	0.131	1.743
NGC 3769	15.2	5.150	–	–	0.601	0.131	0.846	0.253	0.672
NGC 3835	0.0	0.000	–	–	–	–	–	–	–
NGC 3835	-22.0	29.080	–	–	0.460	0.100	–	–	–
NGC 3835	-13.9	13.370	–	–	0.645	0.121	–	–	–
NGC 3835	18.6	31.210	–	–	0.380	0.084	0.254	0.162	1.709
NGC 3976	0.0	0.000	–	–	–	–	–	–	–
NGC 3976	-86.2	55.110	–	–	0.428	0.369	0.255	0.733	1.354
NGC 3976	-42.3	69.950	–	–	0.438	0.039	0.241	0.064	1.788
NGC 3976	-30.4	14.910	–	–	0.455	0.084	0.265	0.149	1.402
NGC 3976	-20.3	7.200	0.092	0.079	0.508	0.089	0.253	0.161	0.822
NGC 3976	20.3	8.620	0.038	0.054	0.491	0.063	0.328	0.113	1.282
NGC 3976	98.0	140.700	0.031	0.276	0.353	0.277	0.287	0.554	1.473
NGC 4047	0.0	4.700	–	–	0.494	0.062	–	–	–
NGC 4047	-27.0	4.470	–	–	0.471	0.063	–	–	–
NGC 4047	-14.5	35.760	0.034	0.038	0.382	0.044	0.370	0.082	1.179
NGC 4047	-9.1	28.740	–	–	0.289	0.027	0.199	0.050	0.948
NGC 4047	-5.9	18.250	–	–	0.319	0.040	0.201	0.073	1.226
NGC 4047	7.1	13.910	–	–	0.293	0.037	0.214	0.070	1.238
NGC 4047	22.4	11.530	–	–	0.543	0.149	0.561	0.287	1.619
NGC 4047	24.7	19.860	–	–	0.391	0.128	0.418	0.248	1.996

Table 5. Parameters of the HII regions (Cont.)

Galaxy	R (")	EW(Hα) (Å)	[OI]/Hα	err([OI]/Hα)	[NII]/Hα	err([NII]/Hα)	[SII]/Hα	err([SII]/Hα)	S1/S2
NGC 4162	0.0	5.720	0.014	0.033	0.660	0.036	0.320	0.067	0.770
NGC 4162	-66.0	200.300	0.024	0.035	0.280	0.039	0.331	0.074	1.098
NGC 4162	-45.5	20.610	0.106	0.088	0.333	0.091	0.474	0.180	1.541
NGC 4162	-39.6	29.920	0.035	0.048	0.349	0.052	0.408	0.101	1.566
NGC 4162	-31.9	27.430	0.025	0.040	0.424	0.045	0.416	0.085	1.409
NGC 4162	-22.1	16.880	0.017	0.032	0.440	0.036	0.299	0.067	1.663
NGC 4162	9.1	11.320	0.028	0.041	0.425	0.045	0.259	0.084	1.241
NGC 4162	12.3	29.460	0.021	0.031	0.378	0.035	0.336	0.065	1.407
NGC 4162	25.4	60.790	0.032	0.028	0.339	0.032	0.266	0.059	1.154
NGC 4284	0.0	1.200	0.096	0.028	0.817	0.290	–	–	–
NGC 4284	-20.3	9.840	–	–	0.676	0.224	–	–	–
NGC 4284	16.9	10.930	–	–	0.429	0.114	0.416	0.216	1.315
NGC 4290	0.0	31.000	0.008	0.014	0.507	0.019	0.266	0.032	1.188
NGC 4290	28.7	11.460	–	–	0.547	0.141	–	–	–
NGC 4290	-23.7	12.100	2.283	0.014	0.521	0.141	–	–	–
NGC 4389	0.0	64.520	0.008	0.011	0.289	0.014	0.247	0.024	1.326
NGC 4389	-49.0	46.280	–	–	0.314	0.067	0.387	0.126	1.438
NGC 4389	-42.3	26.770	–	–	0.386	0.095	0.417	0.177	1.732
NGC 4389	-23.7	49.770	0.009	0.022	0.281	0.027	0.305	0.050	1.350
NGC 4389	-11.8	48.860	0.018	0.023	0.304	0.028	0.279	0.051	1.218
NGC 4389	15.2	19.710	–	–	0.375	0.031	0.393	0.057	1.335
NGC 4389	27.0	35.030	0.022	0.028	0.301	0.034	0.325	0.062	1.485
NGC 4389	54.1	30.860	–	–	0.422	0.060	0.406	0.110	1.271
NGC 4455	0.0	14.190	–	–	0.075	0.158	–	–	–
NGC 4455	-51.0	157.000	–	–	0.055	0.032	0.166	0.065	1.239
NGC 4455	-22.0	58.890	–	–	0.103	0.073	0.301	0.147	2.004
NGC 4455	-8.1	69.550	–	–	0.068	0.033	0.202	0.067	1.266
NGC 4455	25.5	93.720	–	–	0.083	0.036	0.174	0.072	1.870
NGC 4496A	0.0	12.230	–	–	0.397	0.079	0.455	0.153	1.274
NGC 4496A	-112.5	100.800	–	–	–	–	0.371	0.180	0.991
NGC 4496A	-35.1	108.900	0.058	0.028	0.316	0.106	–	–	–
NGC 4496A	-16.3	43.100	–	–	0.300	0.051	0.326	0.099	1.522
NGC 4496A	-10.4	15.590	–	–	0.373	0.066	0.393	0.128	2.025
NGC 4496A	-4.5	7.610	–	–	0.432	0.160	0.768	0.318	1.685
NGC 4496A	11.1	14.210	–	–	0.499	0.092	0.630	0.179	1.304
NGC 4496A	27.3	88.680	–	–	0.251	0.044	0.348	0.087	1.632
NGC 4496A	53.5	400.000	0.030	0.762	0.164	0.762	0.150	1.524	1.641
NGC 4496B	0.0	49.360	0.013	0.017	0.387	0.022	0.261	0.038	1.342
NGC 4496B	-76.0	71.400	–	–	0.222	0.144	0.255	0.286	1.397
NGC 4496B	-60.8	61.260	–	–	0.226	0.053	0.276	0.101	1.389
NGC 4496B	-20.3	26.320	–	–	0.356	0.066	0.341	0.121	1.410
NGC 4496B	16.9	24.270	–	–	0.316	0.070	0.348	0.131	1.321
NGC 4525	0.0	4.600	–	–	0.372	0.137	0.644	0.271	1.364
NGC 4525	-49.0	9.940	–	–	0.328	0.155	0.447	0.303	0.857
NGC 4525	-11.8	4.810	–	–	0.373	0.159	0.643	0.316	0.848
NGC 4525	21.8	13.300	–	–	0.183	0.095	0.424	0.192	1.203
NGC 4567	0.0	6.930	–	–	0.377	0.053	–	–	–
NGC 4567	-42.3	26.270	–	–	0.343	0.054	0.282	0.098	1.101
NGC 4567	-15.2	16.410	–	–	0.232	0.057	0.159	0.105	0.893
NGC 4567	13.5	20.650	–	–	0.378	0.053	0.199	0.093	1.435
NGC 4567	47.3	9.130	–	–	0.474	0.101	0.417	0.188	1.444
NGC 4568	0.0	18.930	–	–	0.368	0.022	0.168	0.040	1.141
NGC 4568	-42.3	22.790	–	–	0.293	0.054	0.272	0.099	0.803
NGC 4568	-20.3	20.230	–	–	0.344	0.041	0.213	0.074	0.916
NGC 4568	-10.1	12.600	–	–	0.421	0.060	0.205	0.107	1.006
NGC 4568	18.6	22.920	–	–	0.339	0.035	0.210	0.064	1.036
NGC 4568	43.9	36.050	–	–	0.315	0.047	0.158	0.082	1.005
NGC 4568	67.6	36.080	–	–	0.349	0.063	0.278	0.113	1.092
NGC 4793	-43.6	88.780	–	–	0.240	0.060	0.284	0.118	0.973
NGC 4793	-33.8	24.280	–	–	0.348	0.059	0.418	0.116	1.252
NGC 4793	-28.6	14.720	–	–	0.334	0.114	–	–	–
NGC 4793	-17.6	122.200	0.005	0.007	0.313	0.009	0.216	0.016	1.215
NGC 4793	21.4	84.770	0.018	0.013	0.344	0.015	0.340	0.028	1.210
NGC 4793	-3.9	20.210	–	–	0.299	0.017	0.222	0.032	1.340
NGC 4793	0.0	8.940	–	–	0.428	0.027	0.258	0.051	1.050
NGC 4793	4.5	32.390	–	–	0.267	0.019	0.193	0.034	1.150
NGC 4793	0.4	25.770	0.020	0.022	0.319	0.025	0.299	0.047	1.167
NGC 4793	26.0	70.110	0.033	0.024	0.324	0.027	0.342	0.050	1.586
NGC 4793	38.4	23.670	–	–	0.211	0.104	–	–	–
NGC 4800	0.0	4.090	–	–	0.634	0.064	0.314	0.120	0.780
NGC 4800	-23.7	12.890	–	–	0.473	0.064	0.339	0.115	1.016
NGC 4800	-10.1	8.320	–	–	0.494	0.063	0.255	0.115	1.098
NGC 4800	5.1	7.140	–	–	0.467	0.043	0.248	0.082	0.951
NGC 4800	23.7	23.660	–	–	0.403	0.038	0.237	0.065	1.342

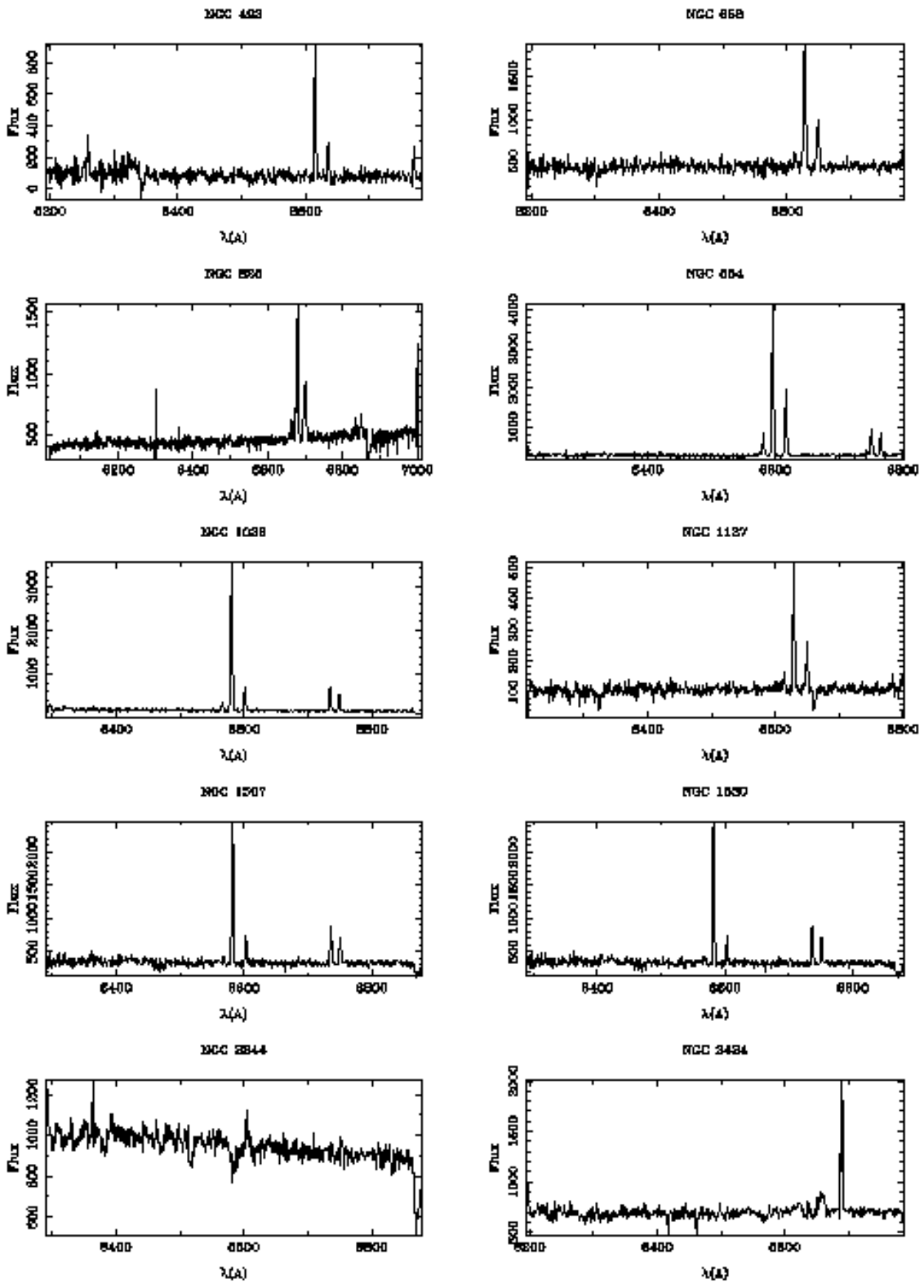

Fig. 21. Nuclear spectra for the whole sample.

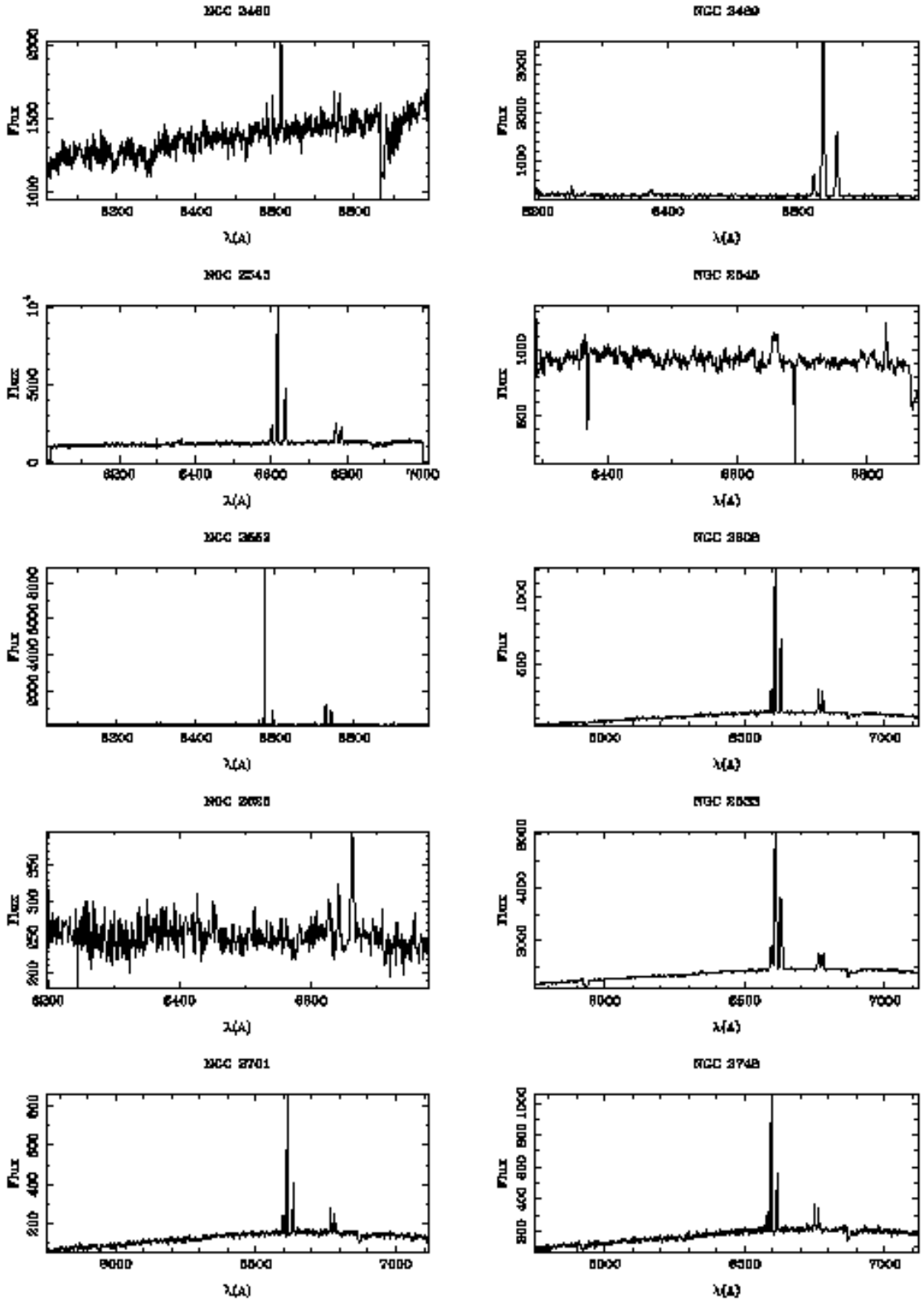

Fig. 21. Nuclear spectra for the whole sample (cont.).

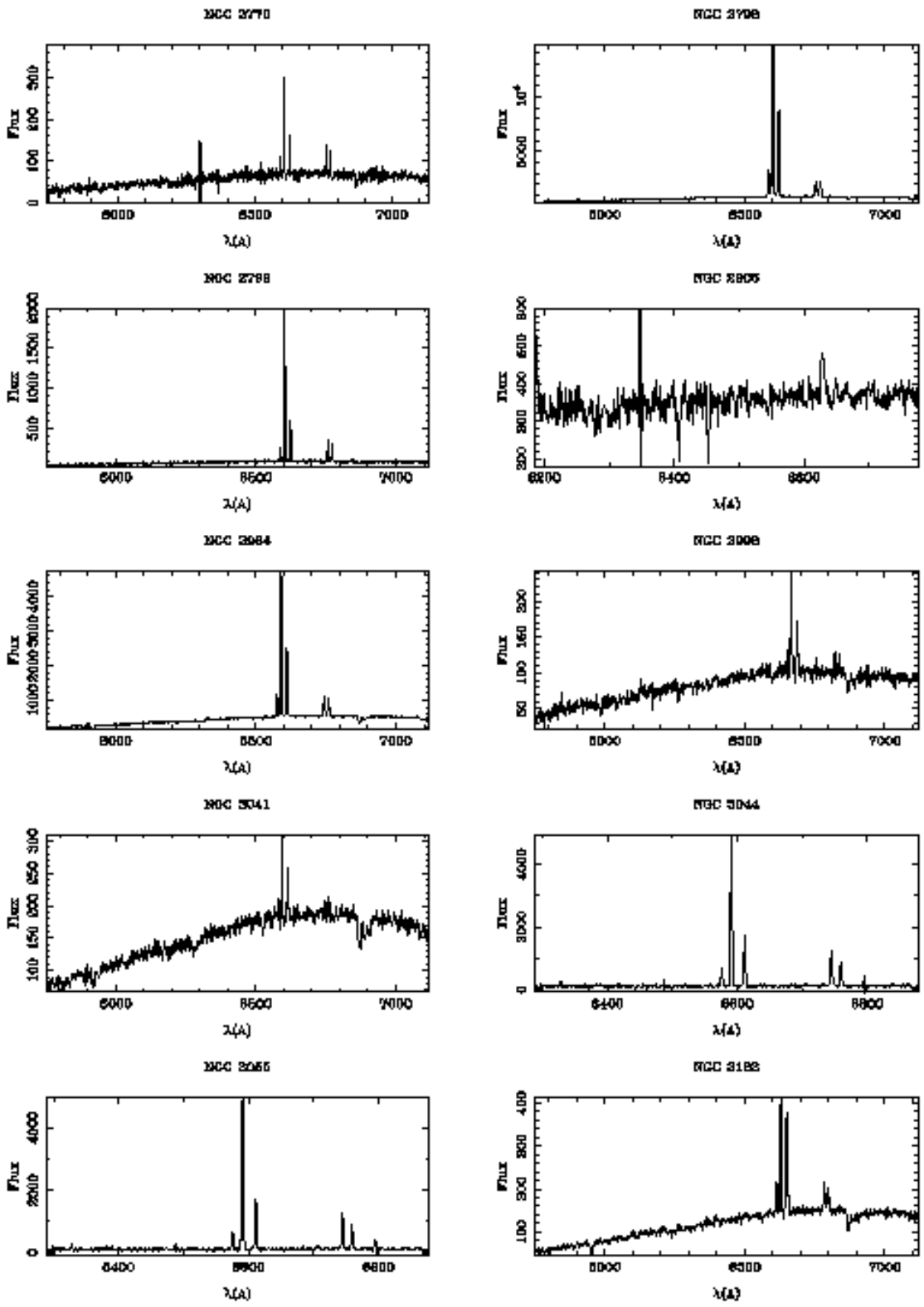

Fig. 21. Nuclear spectra for the whole sample (cont.).

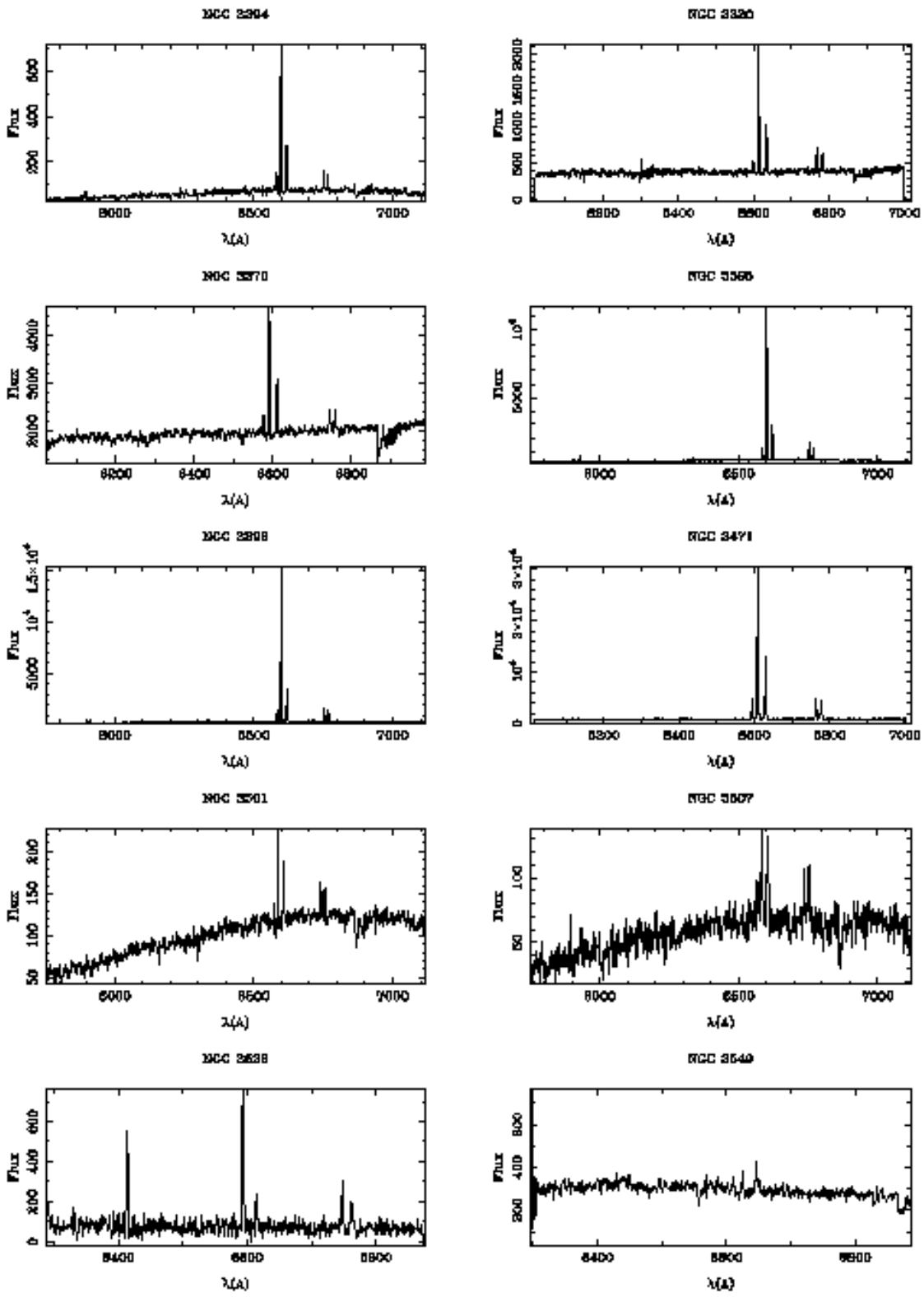

Fig. 21. Nuclear spectra for the whole sample (cont.).

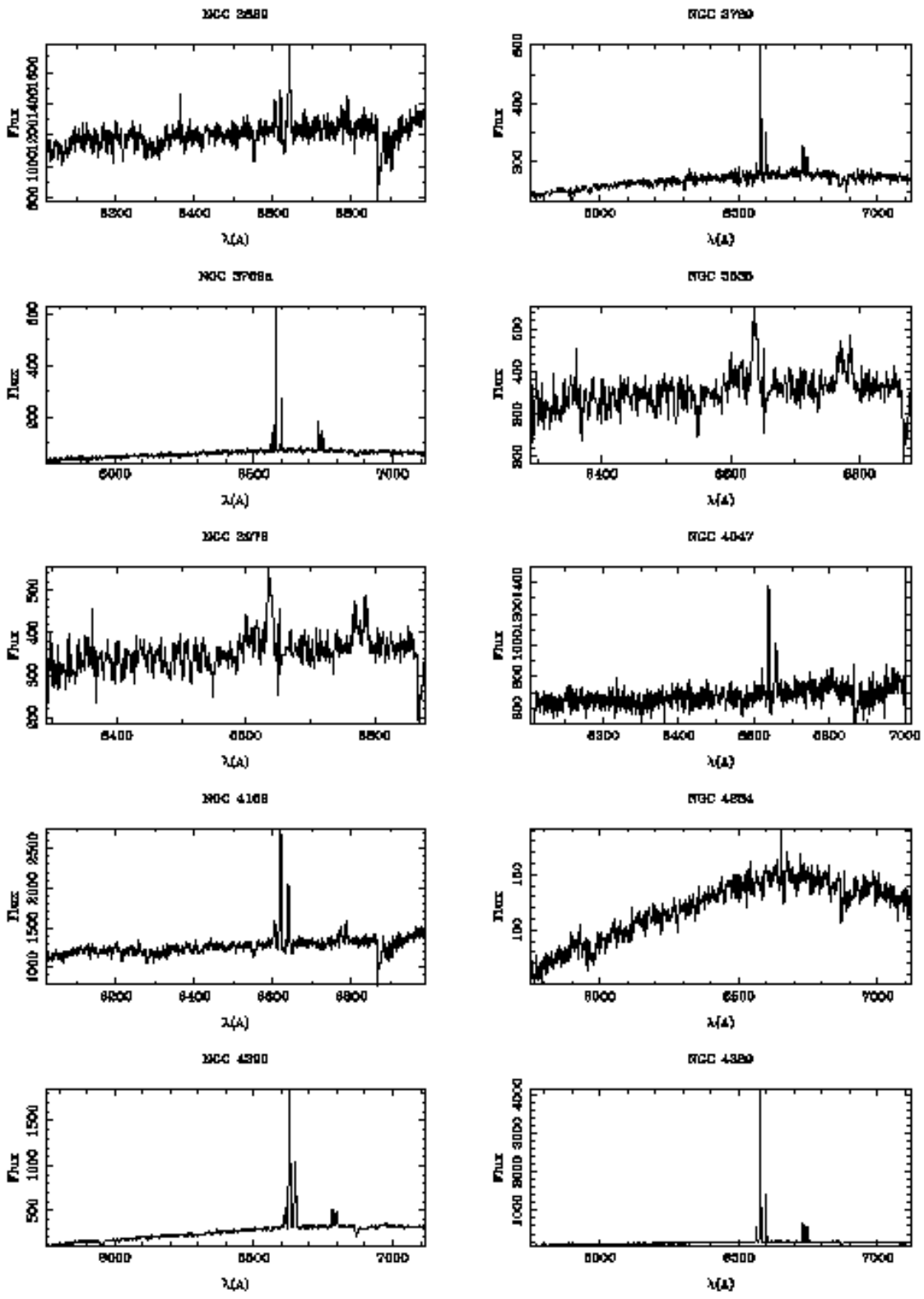

Fig. 21. Nuclear spectra for the whole sample (cont.).

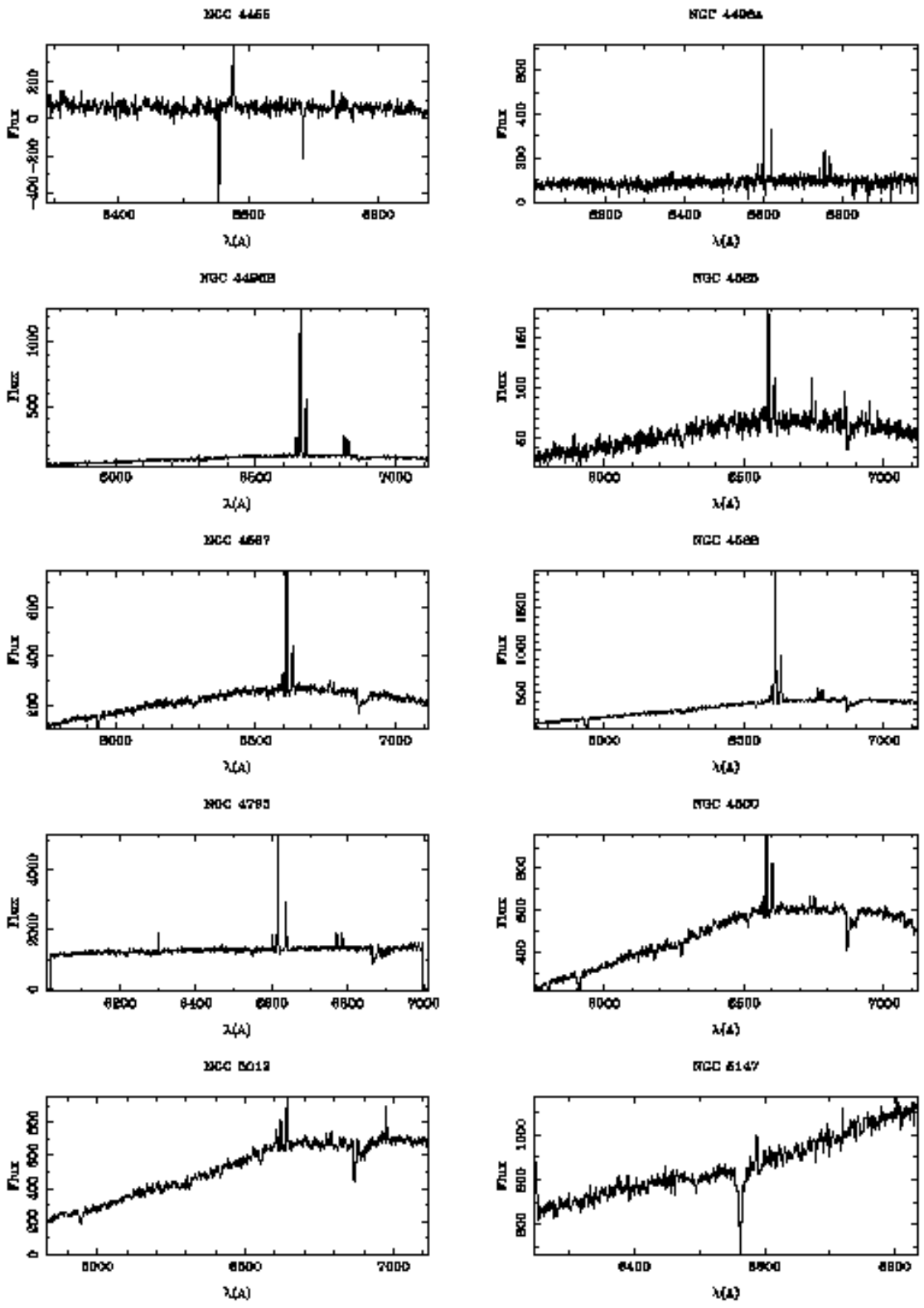

Fig. 21. Nuclear spectra for the whole sample (cont.).

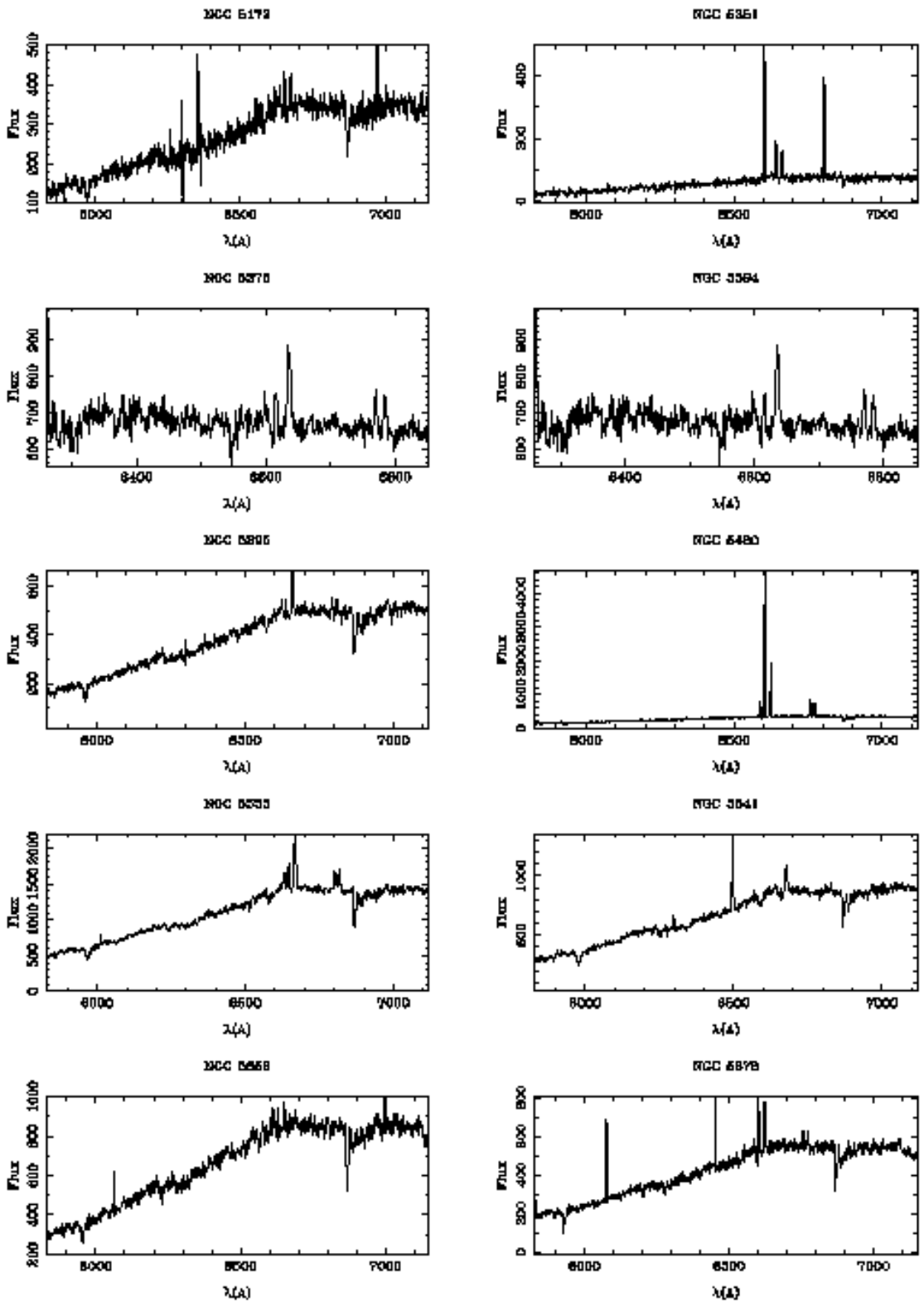

Fig. 21. Nuclear spectra for the whole sample (cont.).

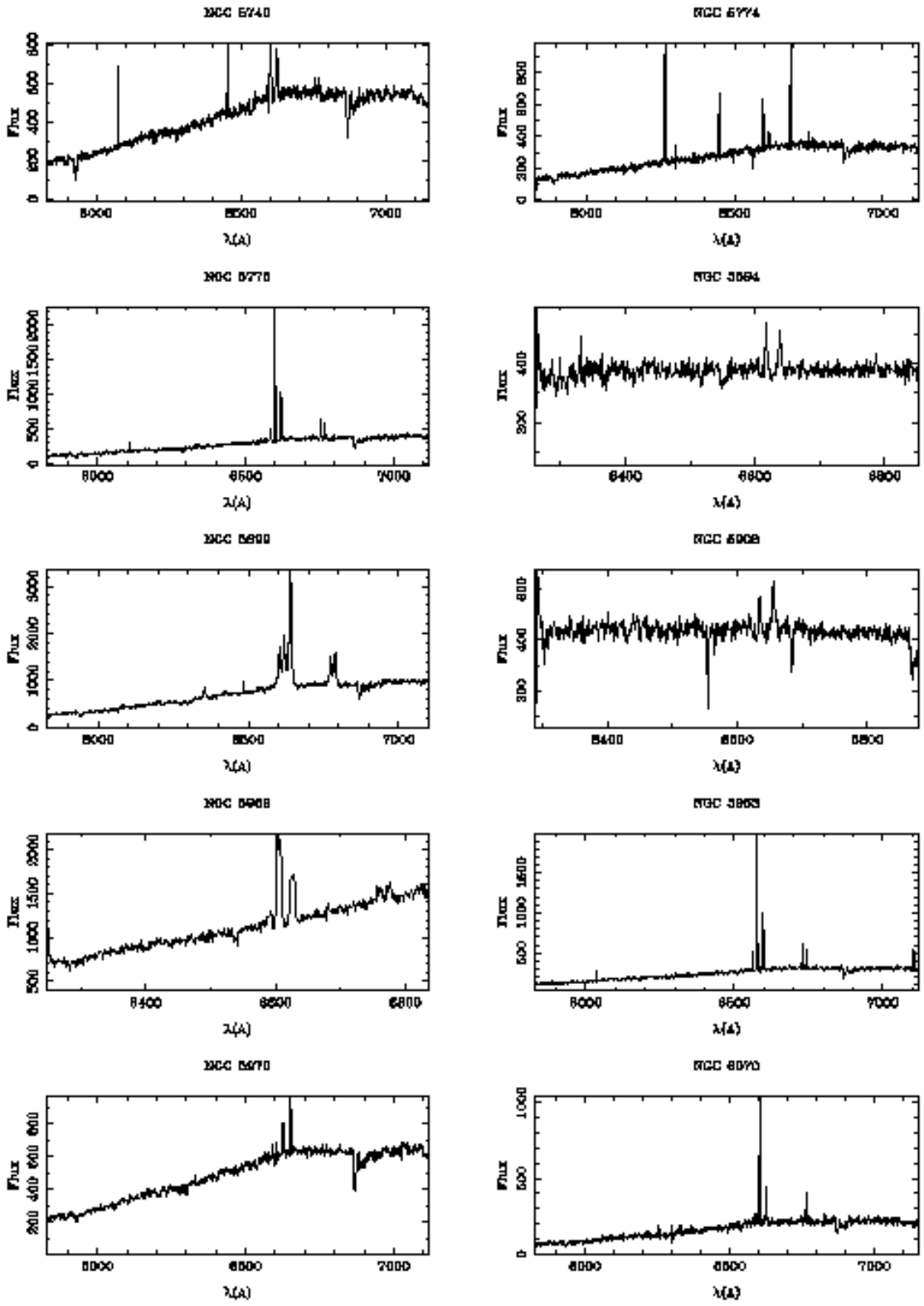

Fig. 21. Nuclear spectra for the whole sample (cont.).

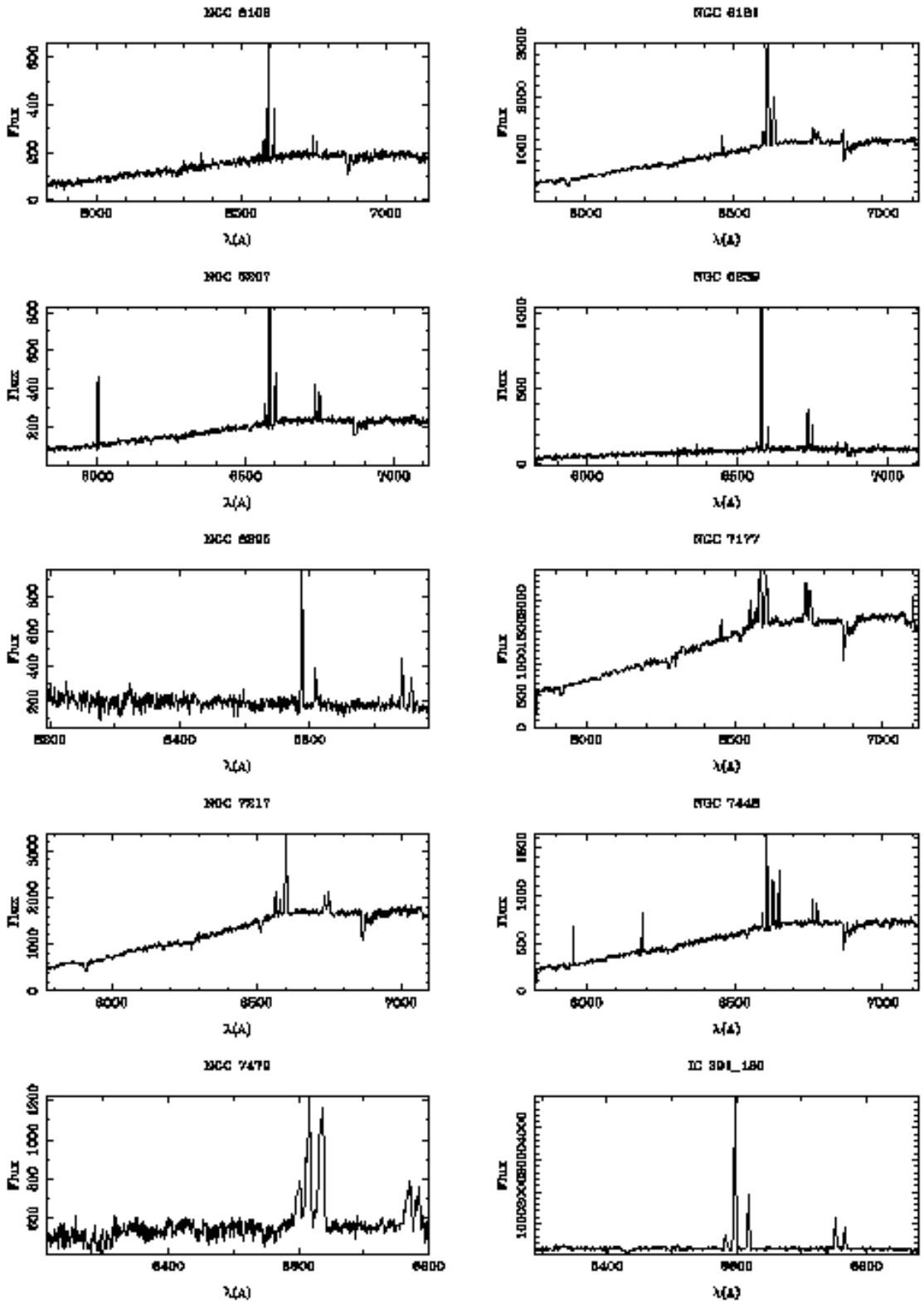

Fig. 21. Nuclear spectra for the whole sample (cont.).

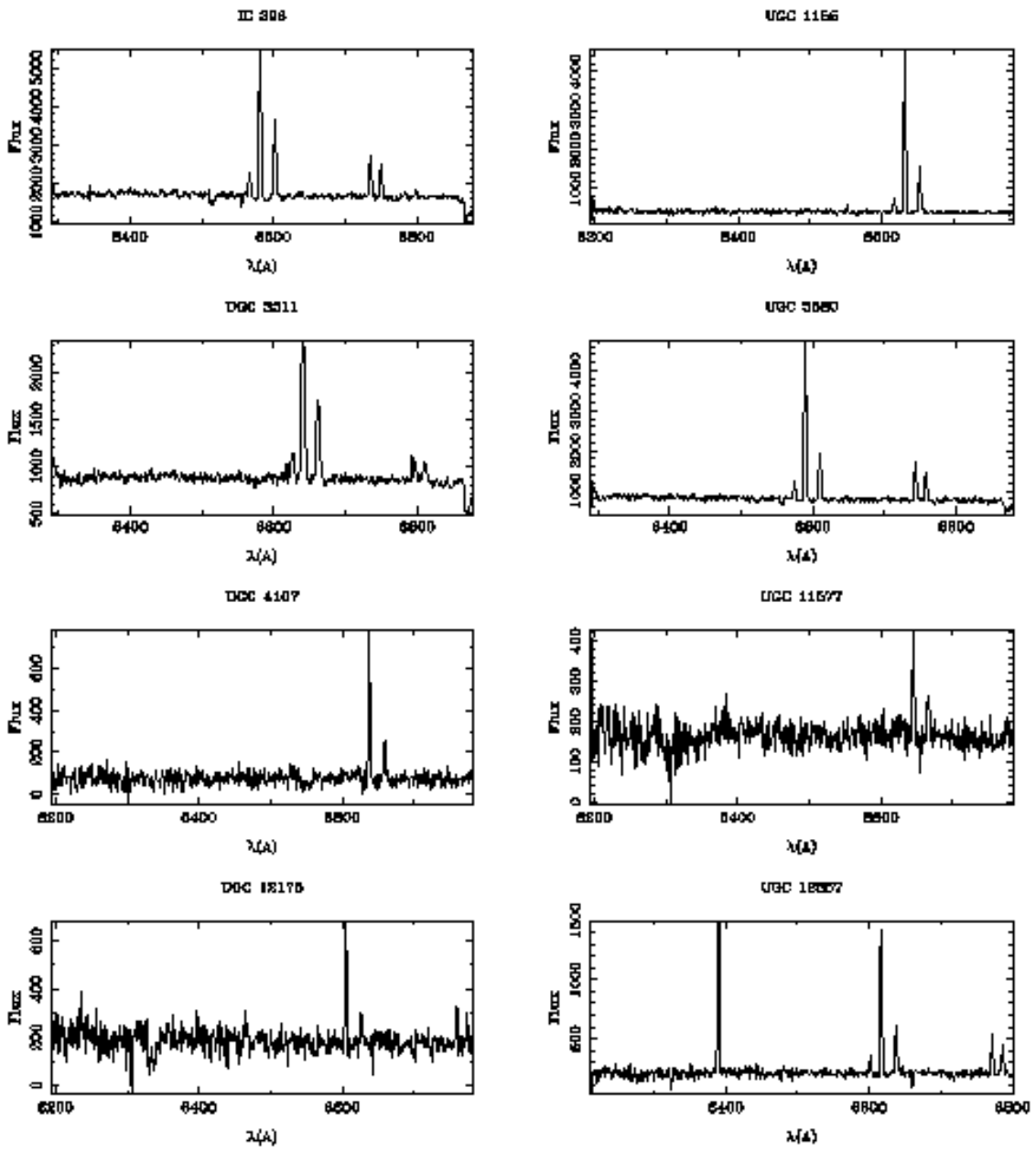

Fig. 21. Nuclear spectra for the whole sample (cont.).